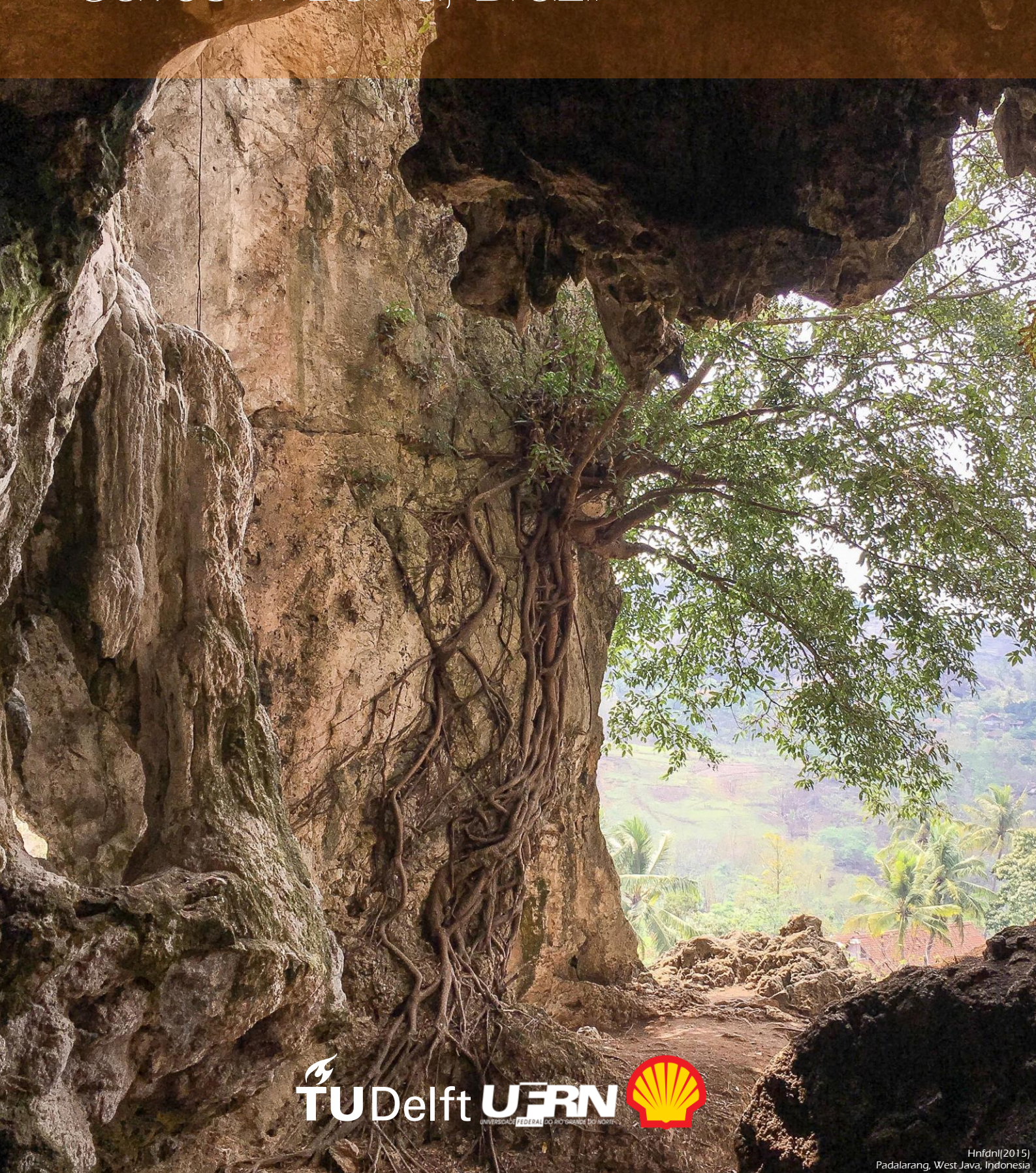


Hanif Dinul Islam

# Geometry and Stability Analysis of Caves in Bahia, Brazil





# Geometry and Stability Analysis of Caves in Bahia, Brazil

By

Hanif Dinul Islam

in partial fulfilment of the requirements for the degree of

**Master of Science**  
in Applied Earth Science

at the Delft University of Technology,  
to be defended publicly on Wednesday August 28, 2019 at 10:00 AM (Room 6,75).

Supervisor:	Prof. Dr. G. Bertotti	TU Delft
Thesis committee:	Drs. J. C. Blom	TU Delft
	Prof. Dr. W. R. Rossen,	TU Delft

An electronic version of this thesis is available at <http://repository.tudelft.nl/>.



*This page is left blank intentionally*

# Preface

بِسْمِ اللَّهِ الرَّحْمَنِ الرَّحِيمِ

The long journey of my Master study is finally coming to an end. Therefore, I would like to express my sincere gratitude to the people who have supported me through ups and downs for the last ten months.

The research was not easy, but conducting extensive investigation has allowed me to explore more about the new things that I have never been thinking about before. Fortunately, I have an excellent supervisor, Prof. Giovanni Bertotti, who was always available and willing to answer my queries. His helpful and constructing character has made me a better person, both personally and academically. I do not regret to choose him as my thesis chairman.

I would also like to thank Stephan de Hoop. His day-to-day guidance safeguarded that I was always on the correct path. I will not forget how the Friday “brain was storming” meeting for the last ten months (also for the *gratis* coffee in every meeting !). You were always happy to answer my many questions; even those are in an “unplanned” meeting elsewhere.

Special thanks to both of my graduation committees, Prof. Bill Rossen & Dr. Jan Kees Blom. Their critical and extensive feedbacks have helped me in completing this thesis as an academically-approved work.

This thesis was in the corporation of UFRN (Universidade Federal do Rio Grande do Norte) and funded by Stichting Molengraaff Fonds (STMF) & Shell Brazil. I am incredibly grateful for their contribution and the trust they put in me. I was once a man who had a bucket list to go to Brazil, but because of this project, I can make my dream come true. This is not only a thesis project but also a bucket list fulfilling.

My warmest thanks are due to my small family in Indonesia for their miles-away lovely support. Their contribution allowed me to achieve the goals that we initially set forth at the beginning of my study. *Terima Kasih Pa, Ma, Dek!*

My gratitude is also protracted to my Indonesian friends, PPI Delft (Indonesian Association in Delft), BP PPID #APRESIASIK, Alstublief 456. Living in Delft will not be the same and easier without you all.

Last but not least, I would not reach this stage without my one call away, +1, Syafira Amanda. 5-6 hours difference, not easy at all I admit, but we have made it!

*Terima kasih banyak !*

*Hanif Dinul Islam  
Delft, August 2019*

*This page is left blank intentionally*

# Contents

Preface .....	iii
Contents .....	v
List of Figures .....	vi
List of Tables .....	viii
List of Symbols & Abbreviations .....	ix
Abstract .....	xi
1. Introduction .....	1
1.1. General Overview .....	1
1.2 Objective .....	1
2. Literature Study .....	2
2.1 Regional Geology .....	2
2.2 Karst in General .....	3
3. Methodology .....	6
3.1 Data Acquisition .....	6
3.2 Alignment of Caves .....	6
3.3 Geometry Analysis .....	7
3.3.1 Shape of the tunnels .....	7
3.3.2 Curve-Skeletons of the caves .....	7
3.3.3 Conduit Orientation .....	9
3.4. Structural Data Analysis .....	9
3.5 Stability Analysis .....	9
4. Results & Discussions .....	13
4.1 Conduit Orientation .....	13
4.1.1 Conduit Orientation Discussion .....	15
4.2 Tunnel Shape & Aspect Ratio .....	15
4.2.1 Geometry Analysis Discussion .....	25
4.3 Structural Data Analysis .....	26
4.4 Stability Analysis .....	27
4.4.1 Base Case .....	29
4.4.2 Real Case (Individual Tunnel) .....	30
4.5 Sensitivity Analysis .....	32
4.5.1 Sensitivity Test – Group Parameters Changes .....	32
4.5.2 Sensitivity Test-Multiple Tunnels analysis .....	37
4.5.3 Sensitivity Test – Spacing Changes .....	40
4.5.4 Stability & Sensitivity Analysis Discussion .....	41
5. Conclusion & Recommendation .....	43
5.1 Conclusion .....	43
5.2 Recommendation .....	43
Bibliography .....	44
Appendices .....	47
Appendix 1 : 5 caves map overview .....	47
Appendix 2 : Detailed Point Cloud Data .....	47
Appendix 3 : Alignment Cave .....	48
Appendix 4 : Structural Data .....	51
Appendix 5 : Stability Analysis Contour Plot .....	55
Appendix 6 : Tornado Plots .....	58

# List of Figures

Figure 1 General geology of Eastern Brazil showing the São Francisco Craton and the location of the Irecê and São Francisco basins. (Misi and Kyle,1994 modified after Dardenne et al 1986) .....	2
Figure 2 Geologic map of The Irecê Basin (Misi And Kyle,1994 generalized after Misi 1979 and Bonfim et al 1985) .....	3
Figure 3 Generalized stratigraphy of The Eastern and Western Margins of The Irecê Basin (Modified after Nascarebhas et al,1984).....	3
Figure 4 Karst and Speleogenesis in the context of diagenetic zones and groundwater flow regimes. (Klimchouk,2012).....	4
Figure 5 A & B are the feeder conduits from artesian caves (join master passages from a side, Klimchouk 2005), C & D are the ceiling cupolas and rising chimneys in Zoloushka Cave (Andreychouk & Klimchouk 2017) and E is the Domepit (Vertrical shaft) in Great Onyx Cave ( Photo by James St.John 2011) .....	4
Figure 6 Conceptual representation of the morphologic suite of rising flow (MSRF), diagnostic of upwelling transverse cave-forming flow and hypogene speleogenesis (Klimchouk,2013) .....	5
Figure 7 Mobile LIDAR Equipment (Hoop & Prabhakaran,2018) .....	6
Figure 8 The Allignment of lap LAP (a) with some adjustment based on the recent map (b) .....	7
Figure 9 The example of the middle point and middle axis in an object.....	7
Figure 10 Visualization of the skeleton creation rules .....	8
Figure 11 Skeleton of TOR.....	9
Figure 12 The Mohr-Coloumb criterion (modified from Goodman,1989) .....	10
Figure 13 The Rose Diagram of DDM represents the conduit orientation.....	13
Figure 14 The Rose Diagram of IOIÔ represents the conduit orientation.....	13
Figure 15 The Rose Diagram of TOR represents the conduit orientation .....	14
Figure 16 The Rose Diagram of LAP represents the conduit orientation .....	14
Figure 17 The Rose Diagram of PAX represents the conduit orientation.....	14
Figure 18 The presence of sediment content that covered the real tunnel base .....	15
Figure 19 The equation for aspect ratio calculation in ellipse shape .....	15
Figure 20 The cross sections & aspect ratio calculations of DDM .....	16
Figure 21 Left : The Aspect Ratio Plot vs Distance (0 m distance starts from the southern part) & Right : The frequency plot of slices of DDM .....	16
Figure 22 The Cross Sections of IOI & Aspect Ratio Calculation .....	17
Figure 23 Left : The tunnel width changes of entire slices (0 m distance starts from the lake position), Right : The frequency plot of IOI calculated aspect ratio.....	17
Figure 24 The Illustration of the water table changes effect to the tunnel shape (after Audra et al., 2019) .....	18
Figure 25 The boundary between eastern part and the western part (dashed line) .....	18
Figure 26 The Details of Cross Sections -TOR (Eastern Vertical Part).....	19
Figure 27 The three mazes part in TOR.....	19
Figure 28 The Details of Cross Sections -The Maze 1 Part .....	20
Figure 29 Cross Sections Of The Eastern Horizontal Part of TOR .....	20
Figure 30 The Details of Cross Section -TOR (Western Part) .....	21
Figure 31 The shape differences between two parts of TOR cave .....	22
Figure 32 The boundary between thin branches of the tunnel (blue dashed square) & the large body tunnel (red dashed square) .....	23
Figure 33 The Shape Comparison between Two Parts - LAP .....	23
Figure 34 The Cross Sections of PAX: Rectangular-Ellipses Shape (Red Coloured Area), Horizontal Ellipses (Green Coloured Area) and Triangular Shape (Blue Coloured Area).....	24
Figure 35 Left : The Aspect Ratio Plot vs & Right : The frequency plot of slices of PAX .....	24
Figure 36 Frequency plots for every tunnel shapes .....	25
Figure 37 Rose Diagram plot of the structural data and the conduit orientation of all caves .....	26
Figure 38 The position map of all the caves + Plotted Rose Diagram .....	27
Figure 39 Input parameters for stability analysis.....	27
Figure 40 The simple ellipse shapes for base case input.....	28
Figure 41 The slices for individual tunnel analysis (Real data) .....	29
Figure 42 Aspect Ratio vs Depth of Failure Plot (Base Case).....	29

Figure 43 Aspect Ratio vs Depth of Failure Plot (Real Case) .....	30
Figure 44 Failure Depth comparison (Base Case vs Real Case (Individual) .....	31
Figure 45 The Mohr Coloumb envelope changes due to changes of cohesion, friction angle & tensile strength	32
Figure 46 Sensitivity Test Results (Rock Mass Strength Changes) .....	33
Figure 47 Sensitivity Test Results (Rock Mass Elastic Changes) .....	35
Figure 48 Sensitivity Test Results (Density Changes) .....	36
Figure 49 The sensitivity tornado plot for all of the parameter changes .....	37
Figure 50 (A&B) The failure contour for the two tunnels analysis, (c): The position of the slices on the map, (d) The scale bar legends (the red colour bar represents the failure and the blue represents the non failure area) .	37
Figure 51 Individual Tunnel analysis vs Two Tunnels analysis Failure Depth Plot .....	38
Figure 52 (A,B&C) The Failure Contour for The Two Tunnels Analysis, (D): The Position of the slices on the map, (E) The Scale Bar Legends (The Red Colour Bar Represents The Failure and The Blue Represents The Non Failure Area) .....	38
Figure 53 Individual Tunnel analysis vs Two Tunnels analysis Failure Depth Plot .....	39
Figure 54 Space Changing effect on failure depth Plot .....	41

# List of Tables

Table 1	The list of tunnels included into the analysis .....	11
Table 2	The Aspect Ratio Calculation of the TOR (western part).....	21
Table 3	Input Data Ranges (Goodman,1989) .....	28
Table 4	Failure Depth for The Base Case.....	30
Table 5	Failure Depth for The Real Case (Individual Tunnel) .....	31
Table 6	The input of rock mass stress changes.....	32
Table 7	Failure depth in respect to rock mass strength changes .....	33
Table 8	The Input of Rock Mass Elastic Changes .....	34
Table 9	Failure Depth in Respect to Rock Mass Elastic Changes .....	34
Table 10	The input of density changes.....	35
Table 11	Failure Depth in Respect to Density Changes .....	36
Table 12	Individual tunnel analysis &two tunnels analysis results .....	38
Table 13	Individual tunnel analysis &two tunnels analysis results .....	39
Table 14	Sensitivity Test -Spacing Changes Results .....	40

# List of Symbols & Abbreviations

<b>DDM</b>	Diva de Maura
<b>IOI</b>	Ioio
<b>TOR</b>	Torrinha
<b>LAP</b>	Lapinha
<b>PAX</b>	Paixao
<b>LIDAR</b>	Light Detection and Ranging
<b>TLS</b>	Terrestrial LIDAR system
$\sigma_h$	Sigma Horizontal
$\sigma_v$	Sigma Vertical
$\nu$	Poisson's Ratio
<b>E</b>	Young Modulus
$\gamma$	Unit Weight
$\rho$	Density of Rock
<b>g</b>	Gravity (9.807 m/s <sup>2</sup> )

*This page is left blank intentionally*

## Abstract

*More than 30% of the world's hydrocarbon reserves are located in carbonate reservoirs, and this percentage is likely to increase, as a result of discoveries of new giant oil fields in carbonate rocks, generically named "Pre-salt layers". However, there are still some problems in understanding karst systems that still unresolved. The karst caves are one of the suitable analogs for karstic reservoirs that also spread all over the world. In this study, the mobile LIDAR (Light Detection and Ranging) data is used to characterize the geometries and to analyze the stability of tunnels under several depths from 5 caves in Bahia, Brazil. The studied caves are representing both of the karstification mechanism (Epigene & Hypogene). In general, there are two tunnel shapes among the caves: horizontal ellipse & Vertical ellipse shapes. Several factors could be controlled the shape origin of the tunnels, but from this study mainly caused by lithology or the geology structure factor. By comparing with the structural data, the conduit orientation generally shows the same trend. Therefore, these conditions suggest a geometrical correlation between the fractures and the caves, and that the observed fractures almost certainly acted as conduits for fluid flow. The stability analysis showed that the vertical ellipse tunnels are more stable compared to the horizontal ellipse. However, all of the tunnels are already unstable in shallow depth (on average less than 2 km depth). The sensitivity tests show several parameters that would affect the stability: Rock Properties (Rock Mass strength, Rock mass elastic, density), number of tunnels in the system and the distances between multiple tunnels.*

**Keywords:** Carbonates, LIDAR, Point Cloud Data, Karst Caves, Stability Analysis

*This page is left blank intentionally*

# Introduction

## 1.1. General Overview

Karst features show a close relationship with tectonic structures (Klimchouk,2000). Fractures and folds have been identified as essential features influencing fluid migration and karst development in carbonates units (Klimchouk and Ford, 2000). Despite advances in the understanding of structural controls on Karst, several problems are still unresolved. Although published predictive models of the origin of cave systems exist, the limited number of field-based investigations makes it challenging to assess the development of Karst (Billi et al., 2007). First, a structural analysis at the scale of the karst system lacks in many studies. Such studies of vast caves, especially of hypogene origin, are rare. Second, it is still a matter of debate as to why some tectonic structures are more vulnerable to karst development than other structures. Third, the correlation of karst patterns with regional deformation has not been addressed previously. Fourth, in the case of hydrocarbon reservoir studies and despite the use of some quantitative assessment and statistical descriptions, detailed and sub-seismic analysis of the deformation-karstification relationship is still lacking (Sauro et al., 2013).

The carbonates host commercial oil accumulations at some essential oil fields. Furthermore, it also believed that karsts are also present in subsurface carbonates reservoirs, such as the sub-salt play offshore Brazil (Pre-salt), where large karst tunnels control the effective permeability (Bruhn et al., 2017; Cazarin et al., 2016). The karst caves are one of the suitable analogues for karstic reservoirs that also spread all over the world. Complex in origin and very strong in heterogeneity, this kind of reservoir is challenging to predict (Xinsong et al., 2019).

Understanding how the karstification process has affected the carbonates' reservoir properties is essential for future exploration (Basso et al.,2018). Apart from enhancing production, these high porosity zones also prove to be significant and unpredictable drilling hazards (thief zones). In this case, Karst poses significant hazards for constructions due to the high probability of collapse and subsidence caused by sinkholes. Additionally, most of these features fall below the seismic resolution, making it hard to predict their geometry and position accurately.).

## 1.2 Objective

This study aims to get an overview of the geometry from all the caves using the only available primary data (point cloud) from the LIDAR survey. The geometry analysis will enable us to observe and analyze the geometries of these caves in the first place. Thus the 3D model data of the cave interiors which acquired through the LIDAR data can be helpful to see what are the shapes of the tunnel that appear inside the cave, which is impossible to see from the aerial / map view perspective. This results will be helpful to see the pattern, how are they are changes and at the end we will try to link it with several factors (lithology/structural geology). Through the results of the geometry analysis, the stability analysis can be done on the various shapes that already occupied. Some parameter changes also can give an idea of how cave stability will be under a specific condition (Depth, Rock Properties, Number of tunnels, Distances). This study can be the first step to answer all of the problems and to see the pattern related to the karst system.

# Literature Study

## 2.1 Regional Geology

The study is located in the Irecê Basin, which is positioned inside the northern part of the São Francisco Craton (SFC) (Bahia, NE Brazil) which is a 910,000 km<sup>2</sup> great platform developed during the late Proterozoic (Karfunkel and Hoppe, 1988). Because of their extent and well-preserved sedimentary sequences, the SFC craton provides relevant records of late Proterozoic sedimentary environment (Misi and Kyle, 1994). The São Francisco Craton is bordered by the fold belts of Aracuai, Brasília, and Sergipano, on the Southeast, West, and Northeast respectively. During the Brazilian orogeny, most of the contractional deformation affecting the SFC was localized in the mountain belts surrounding the São Francisco Craton. However, far-field stresses changed the Neoproterozoic sedimentary cover within the craton interior, where outcropping rock formations exhibit two main phases of deformation, namely: 1) NNE-SSW and 2) E-W striking folds and thrusts (Cruz & Alkmim, 2006; Ennes-Silva et al., 2016).

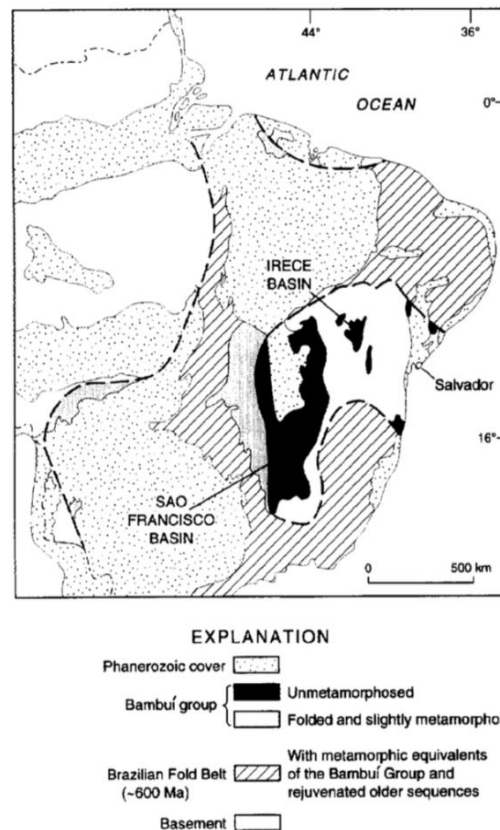


Figure 1 General geology of Eastern Brazil showing the São Francisco Craton and the location of the Irecê and São Francisco basins. (Misi and Kyle, 1994 modified after Dardenne et al 1986)

The Irecê Basin is a relatively small and isolated basin which is the basin widespread within this sedimentary terrane that is dominantly filled by carbonate strata of the Una Group (Misi and Kyle, 1994, Figure 4 & 5). Post-Brazilian orogeny sediments are absent within the Irecê basin, either due to non-deposition or erosion. The Irecê basin contains a basal siliciclastic sequence (The Bebeduoro Formation) composed of diamictites dominantly of glacial origin that also consists of Arkosic quartzite, conglomerate and it is overlain by lacustrine carbonate system. These are succeeded by the Una Group, a marine carbonate sequence in hundred meters thick. The marine units consist of basal laminated limestone and dolomitic limestone sequence that grades upward into dolostone and cherty dolostone with gray argillaceous limestones, shales, siltstones as the middle sequence and

black organic-rich grainstones in the upper sequence (Misi and Kyle, 1994). The generalized stratigraphy of the Irecê Basin is presented in figure 3.

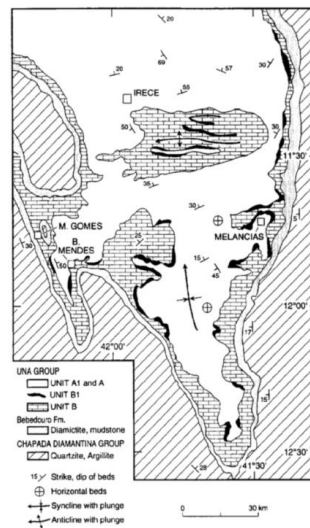


Figure 2 Geologic map of The Irecê Basin (Misi And Kyle, 1994 generalized after Misi 1979 and Bonfim et al 1985)

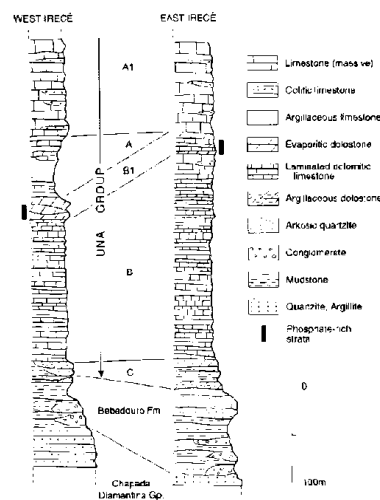


Figure 3 Generalized stratigraphy of The Eastern and Western Margins of The Irecê Basin (Modified after Nascarebhas et al, 1984).

## 2.2 Karst in General

The formation of karst, commonly denoted to as karstification, is triggered by water-rock interactions, hydrogeological mass transport and destruction of permeable soluble rocks (Dreybrodt, Gabrovšek, & Romanov, 2005). The karst paradigm was shifting during the last decades, and the conception of karst has been well-defined from a different standpoint. Some of the perspectives are made by the latest study to characterize the karst system. Regardless the approach, it was recognized that most of the specific properties identified to karst owe their origin to the development of organized dissolution porosity/permeability structures in soluble rock, in other hand karst is a function of speleogenesis (Klimchouk et al. 2000). Two fundamental types of speleogenesis, hypogene, and epigene are determined mainly by distinct hydrodynamic characteristics of the parent groundwater flow system. They distinguish due to variances in hydraulic boundary conditions, geochemical and physical conditions of corresponding speleogenetic domains, hydrodynamic regimes of groundwater (fluid) flow and speleogenesis, and evolutionary trajectories of relevant karst systems (Klimchouk 2015).

Therefore, two major genetic types of karst are defined within the upper part of the Earth's crust: Hypogene and Epigene. The former develops in intimate interaction with the landscape, with both surface and underground components (un-confining conditions) formed by downward-moving CO<sub>2</sub>, consuming meteoric water that generally known as the epigenic karst. Hypogene speleogenesis is defined as the formation of solutionally enlarged permeability structures by the upwelling groundwater flow, independent of recharge from the

overlying or immediately adjacent surface (Klimchouk 2015). Hypogene speleogenesis is associated with an the upwelling flow characteristic of discharge regimes of deeper (subregional and regional) meteoric flow systems, either terminal or intervening, or those of basal flow systems (Figure 4). (Klimchouk 2012).

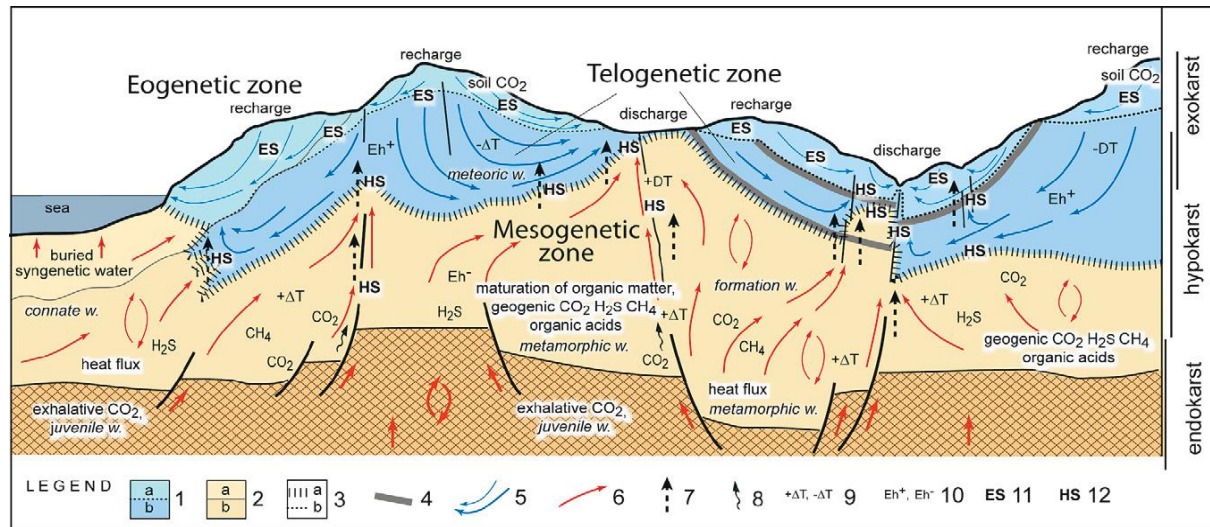


Figure 4 Karst and Speleogenesis in the context of diagenetic zones and groundwater flow regimes. (Klimchouk, 2012)

In contrast to epigene karst systems that develop in intimate interaction with the landscape and have both surface and underground components, hypogene karst evolves without direct genetic linkage with the surface, being initially represented exclusively by void-conduit systems at depth (Klimchouk, 2017). Hypogene caves also characterized by expressed morphological singularities (Klimchouk, 2007) but some forms typical for hypogene caves common for epigene karst. Specific and diagnostic for hypogene caves is that characteristic morphs regularly occur in spatially and functionally related groups where ascending fluid-flow currents, including buoyant convection flow components, can be recognized from solutional sculptures and traced from rising inlet conduits (feeders) to spherical ceiling pockets (cupolas) and outlet features (domepits) (see Figure 5). This regular combination has been distinguished as the morphologic suite of rising flow (MSRF; Klimchouk, 2007, 2009). The characteristics of MSRF is presented in Figure 6. Hypogene karstification involves diverse dissolution mechanisms (Klimchouk 2012), operating either in combination or sequentially in time and space. The depth limit for hypogene speleogenesis is challenging to establish, but based on the latest research (Klimchouk, 2017) suggest that it operates within at least several kilometres.

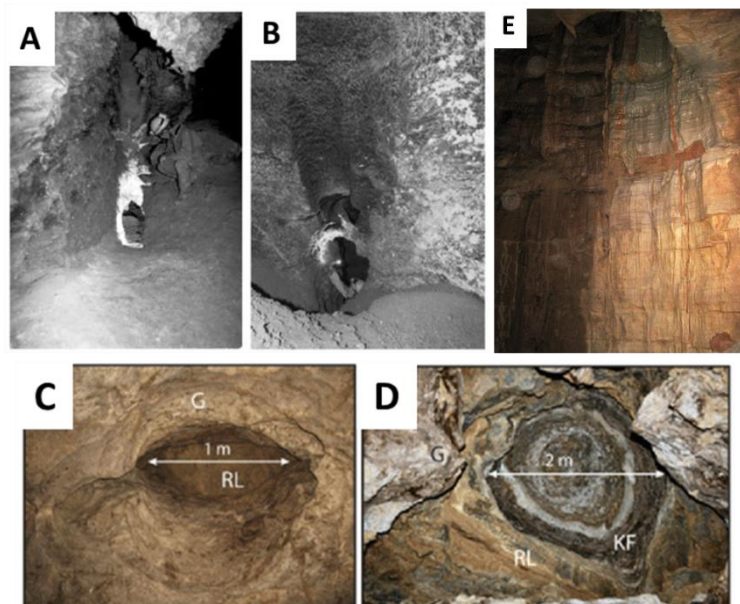


Figure 5 A & B are the feeder conduits from artesian caves (join master passages from a side, Klimchouk 2005), C & D are the ceiling cupolas and rising chimneys in Zoloushka Cave (Andreychouk & Klimchouk 2017) and E is the Domepit (Vertical shaft) in Great Onyx Cave (Photo by James St. John 2011)

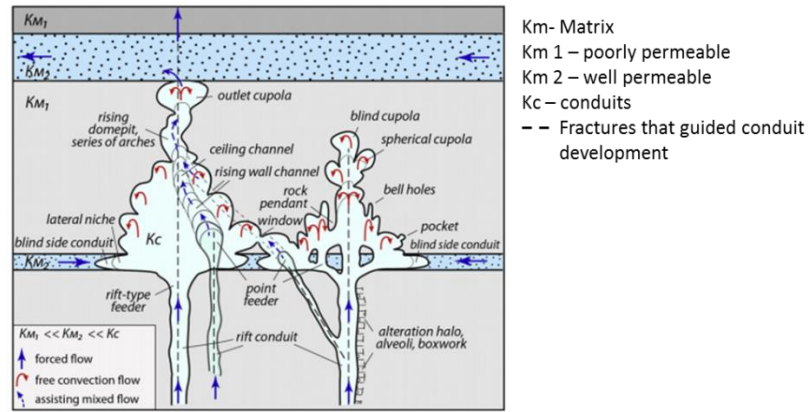


Figure 6 Conceptual representation of the morphologic suite of rising flow (MSRF), diagnostic of upwelling transverse cave-forming flow and hypogene speleogenesis (Klimchouk, 2013)

### 3.1 Data Acquisition

In this study, the geometry analysis of the caves is built using the LIDAR data taken from the fieldwork back then in 2018. All of the caves are located in Bahia, Brazil, which a north-eastern Brazilian state. The exact position of all the caves can be seen in appendix 1. In total six caves LIDAR data are occupied, but only five caves namely *Diva de Maura (DDM)*, *Ioio (IOI)*, *Torrinha (TOR)*, *Lapinha (LAP)* and *Paixao (PAX)* that processed in this study. The other cave, *Lapa de Morro Vermelho* is being processed in the other project.

The fieldwork was focussed on quantification of the morphological features of karsts caves in Brazil using 3D LIDAR (Light Detection and Ranging). During the fieldwork, we used mobile LIDAR technology (ZEB-Revo GeoSLAM). Compared to the terrestrial LIDAR system (TLS), mobile LIDAR has the advantage that user can transverse complex cave passages while simultaneously capturing 3D point clouds of the passage geometry without the need for unwieldy setup and movement of apparatus. Likewise, the intricate and tortuous passages that are common in cave terrain makes it difficult or near impossible to use TLS.



Figure 7 Mobile LIDAR Equipment (Hoop & Prabhakaran, 2018)

The ZEB REVO captures raw laser ranging measurements and inertial data to generate real-time point clouds while the operator is moving through the cave terrain. The portable MMS comprises a laser range scanner coupled to an inertial measurement unit (IMU) mounted on a rotating drive. The rotation of the scanning head produces the third dimension, necessary to generate 3D data. The device uses a 3D SLAM (Simultaneous Location and Mapping) algorithm (Bosse et al., 2012; Zlot and Bosse, 2014b) to fuse the 2D laser scan data with the IMU data to generate the 3D point clouds (GeoSLAM, 2017). This modern data acquisition technique can also help to possibly constrain different types of uncertain manual measurements (e.g., compass) of planar features such as fractures and bedding orientation. Initialization of the device is performed at a fixed location that marks the beginning of the planned trajectory. Initialization of the device is performed at a stationary position that marks the beginning of the intended path. Initialization of the device is performed at a fixed location that marks the beginning of the planned trajectory. The raw data is transferred out from the data logger for further processing to a laptop using a USB stick (Hoop & Prabhakaran, 2018).

After the acquisition, there are more than 35,000,000 points for each cave that had successfully acquired. The point cloud details can be seen in appendix 2.

### 3.2 Alignment of Caves

The main challenges in acquiring the data were primarily related to the accessibility of some locations in the caves, particularly in the vicinity of sudden steep changes in elevation where both hands were required to proceed safely. This condition led to splitting the caves up into more surveys, which eventually led to increased complexity in processing the data (point cloud registration steps). Because of those reasons, some caves need a

manual adjustment to align all of the data. We made the comparison with the original map that has been made by Grupo Bambuí de Pesquisas Espeleológicas (Local speleological surveyor-Brazil). “Cloud compare” software is used to process the raw file from the LIDAR data. The complete result of the alignment of all caves can be seen in appendix 3. The point cloud data also oriented and scaled as the real world condition.

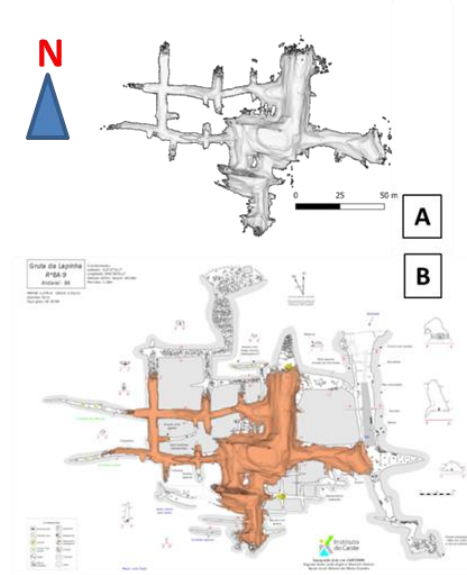


Figure 8 The Alignment of lap LAP (a) with some adjustment based on the recent map (b)

### 3.3 Geometry Analysis

#### 3.3.1 Shape of the tunnels

Using *Cloud compare*®, we can slice the 3D model of the cave into several parts using cross-section tools. By using those tool, we can see the particular shape of tunnels in all of the caves. Each of the cross-section can be saved into *ASCII* text file which a general file type that easy to be imported into other software.

#### 3.3.2 Curve-Skeletons of the caves

Curve-skeletons are thinned 1D representations of 3D objects useful for many visualization tasks (Cornea et al.). During this process, we would like to present the cave (3D) as the representative 1D line using the curve-skeleton creation. We take a middle point to make a medial axis to make a skeleton. In 2D, the medial axis of a shape is a set of curves defined as the locus of points that have at least two closest points on the boundary of the shape (Lieutier et al.). Figure 9 shows the visualization of the middle point and middle axis on an object.

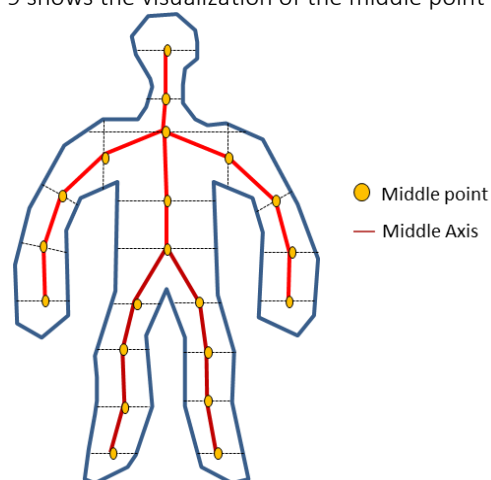


Figure 9 The example of the middle point and middle axis in an object

Several curve-skeleton properties needed to be a valid representative of the whole object/model (Cornea et al.) :

1. *Homotopic (Topology reserving)*

The curve-skeleton should be topologically equivalent to the original object. Preservation of topology can be stated simply as two objects have the same topology if they have the same number of connected components, tunnels and cavities.

2. *Reconstruction*

The curve-skeleton needs to be able to recover the original object.

3. *Thin*

Curve-skeletons should be one-dimensional and must be as simple as it could. Thinness and reconstruction are two conflicting properties, then some of the user-adjustments are needed.

4. *Centred*

An essential characteristic of a curve skeleton is its centeredness within the object. It is required for the curve-skeleton to lie on the medial surface (in 3D) to achieve perfect centeredness since the medial surface is centred within the object.

5. *Connected*

Connected is a consequence of homotopic. If the curve-skeleton corresponds to a single connected object, then by maintaining the topology of this object, the curve-skeleton would have to consist of a single connected component itself.

To be able to fulfil all of the properties above, then during this study, we used two major rules as the basis to make a curve-skeleton for every cave. The rules are as follow :

1. If the length of the branch is less than 10 % of the main tunnel's length, no new skeleton segment needed.
2. If there is a change in the angle of orientation more than 5 degrees, the new skeleton is needed.

The two rules above will produce a more straightforward skeleton but still not change any properties of the cave (e.g., conduit orientation) and the essential features of the cave also still can be seen. See figure 10 for the more detail visualization of the two rules above.

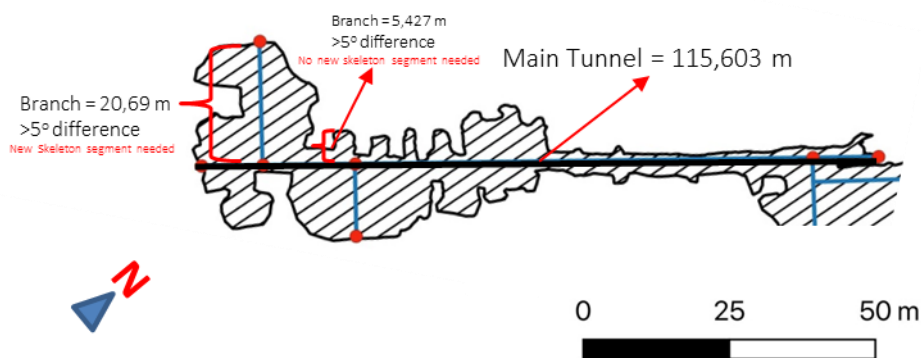


Figure 10 Visualization of the skeleton creation rules

All of the cave skeletons are done using QGIS© software. The input was the ASCII file that extracted from Cloud Compare© software. All of the inputs must be digitized first using the polygon tool in the QGIS©, and all of the projection in the software must be set to WGS84-Pseudo Mercator. The benefit of using this projection is much simpler to calculate, saving many computing cycles, and it will result in a number in meter unit.

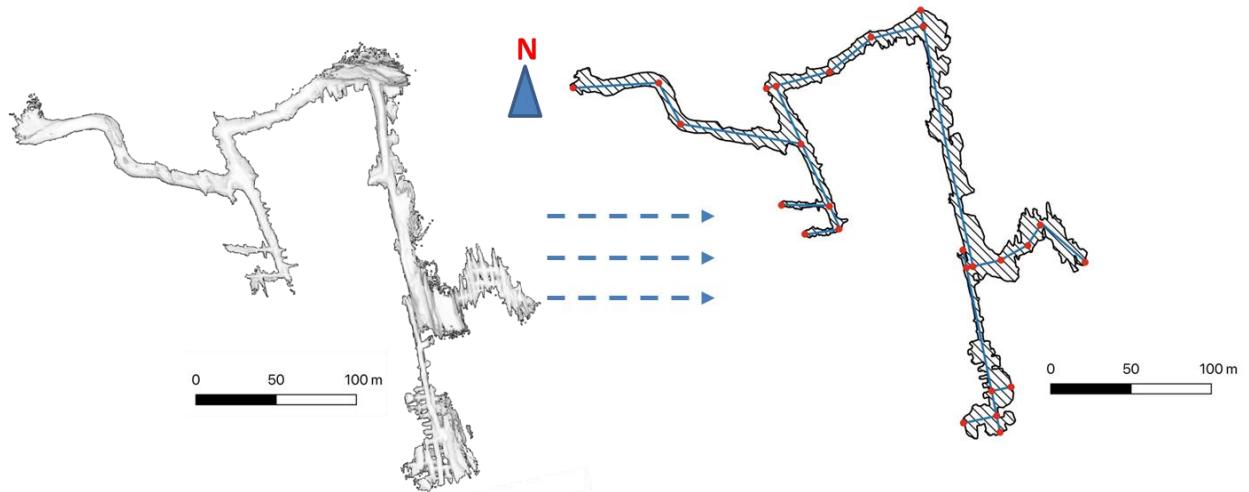


Figure 11 Skeleton of TOR

### 3.3.3 Conduit Orientation

Numerous geological features establish natural drains for underground fluids and consequently strongly impact the development of karstic conduits. Fractures count among those main features (Palmer,1991). Fractures are generally organized into families of particular orientation depending on the regional stress field (Beekman et al.,2000). As a result, karstic networks that are mainly developed along the prominent fractures will show a network pattern (Palmer,1991).

Typically, the data of the orientation are analyzed with a Rose Diagram to represent azimuth. Therefore, to compute the Rose Diagram, each orientation value has been weighted by the length of the edge projection on the horizontal plane (Skeleton). Conduit orientation is thus an interesting parameter for detecting the geological features of influence and for better understanding the speleogenetic processes that have locally dominated. In this way, the entropy of orientations constitutes a useful metric to quantitatively assess the existence and relative importance of preferential karstic developments. The measured orientations are based on the skeleton for each cave. The results assumed as the representation of the whole part of the cave.

All of the conduit orientations are generated from the skeleton that has been made before. All of the processes are using the Line direction histogram plugins in *QGIS*® that visualizes the distribution of line segment directions as a Rose Diagram (weighted using the line segment lengths). We use 10 number of bin for the precision Rose Diagram plotting.

## 3.4. Structural Data Analysis

Beside the LIDAR acquisition, some structural data are also measured from the field (2018) for each of the caves. All of the data are imported into the *Stereonet*® to be converted into a Rose Diagram. Hence, the strike of the fractures can be known, and it is comparable with the conduit orientation that already measured before. All of the measured structure data can be seen in appendix 4.

## 3.5 Stability Analysis

This analysis targets to give an approximation of the depth of failure from each tunnel in each cave. We used several numbers of shapes and saw how deep they could go before the collapse. Some parameters also changed to see the effect from changing of a parameter to the stability of the tunnel. During this analysis, we assumed that all the slice of tunnels is empty/dry. There is no infill factor (fluids/breccia) that take into account on this experiment.

There are numerous methods to analyze the stability of the cave. During this study, the *Examine 2D*® software is chosen since it is the most straightforward software, and it is good to give the first idea of the cave stability in several conditions. The *Examine 2d*® software is a two-dimensional boundary element method (BEM) program for the elastic stress analysis of underground excavations. The BEM is a numerical technique for solving initial value problems based on an integral equation formulation (Beskos 1987). The boundary element method has

been demonstrated to be a viable alternative to the finite element due to its features of boundary-only discretization and high accuracy in stress analysis (Cruse 1996). The integral representation obtains the displacement field in terms of boundary values, and the equation is solved numerically. Boundary values are used to determine displacements and tractions at any interior point of interest (Beskos 1987). This method was applied to various engineering application such as foundation engineering, dynamic soil-structure Interaction, wave propagation, and any other purposes. The elastic boundary element analysis in *Examine 2D* dictates that the material being modelled is assumed to be homogeneous, isotropic, and linearly elastic.

The stability of the caves is presented by the strength factor contour produced by the software. Strength factor itself represents the ratio of material strength to induced stress, at a given point. The strength factor is related to the Mohr-Coloumb theory, which is the simplest and best-known criterion of failure for rocks. The Mohr-Coloumb consists of a linear envelope touching Mohr's circle representing critical combinations of principal stresses, and the material will be failed (figure 12). It stated in terms of normal and shear stresses on the plane described by the point of tangency of a Mohr-Circle with the envelope :

$$\tau_p = S_i + \sigma \tan \theta$$

$\theta$  is called the angle of internal friction, which describes the rate of increase of peak strength with normal stress.  $\tau_p$  is the peak shear stress, or shear strength while  $S_i$  is the constant of the rock or also known as cohesion number. Each type of rock has its failure envelope, and it is found experimentally by fracturing samples of the rock under differential stress.

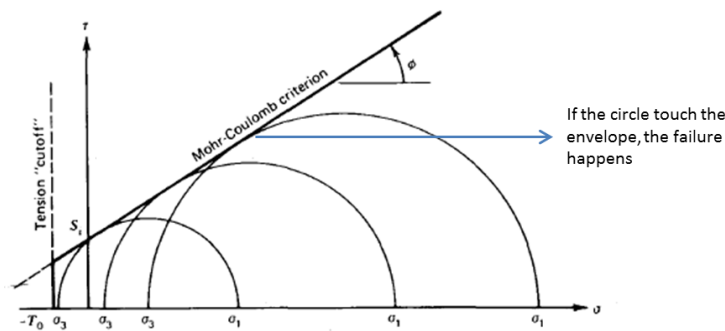


Figure 12 The Mohr-Coloumb criterion (modified from Goodman, 1989)

In the software, the material will be failed if the strength factor value is less than 1 at a given point, which indicates that the stress in the material exceeds the material strength. Since the software only specifies the fail for a singular point on the boundary, we decide to put a threshold of **10% failure points** of each tunnel as **the desired failure depth**.

In total, 19 slices are chosen to be analyzed in this step. Those slices represent the shape of the tunnel from each of the cave. The list of the slices can be seen in table 1.

Table 1 The list of tunnels included into the analysis

CAVE	SLICE
DDM (2)	SLICE 3
	SLICE 4
	SLICE 6
IOI (3)	SLICE 6
	SLICE 7
TOR (4)	SLICE 1 (MAZE PART)
	SLICE 2 (MAZE PART)
	SLICE 3 (MAZE PART)
	SLICE 1.3 (EASTERN VERTICAL PART)
	SLICE 1.5 (EASTERN VERTICAL PART)
	SLICE 3.1 (EASTERN VERTICAL PART)
	SLICE 4 (WESTERN VERTICAL PART)
	SLICE 1 (MIDDLE HORIZONTAL PART)
	SLICE 3 (WESTERN HORIZONTAL PART)
	SLICE 2 (TOP WESTERN PART)
LAP (5)	SLICE 4
	SLICE 6
PAX (6)	SLICE 3
	SLICE 6

*This page is left blank intentionally*

# Results & Discussions

## 4.1 Conduit Orientation

### *DDM (Diva de Maura)*

The Diva De Maura cave is located in the municipality of Seabra, in the state of Bahia, Brazil. The cave comprises of large halls separated by constricted ducts with low ceilings (Hoop & Prabhakaran, 2018). Diva de Maura is one oriented cave if we see from the 2D map. The Rose Diagram also represents the domination of NNW-SSE direction, which is fit with the recent map (in total around 270 m of skeleton length that has the same length with the dominant trend). The visualization of the Rose Diagram and the 2D map can be seen in figure 13.

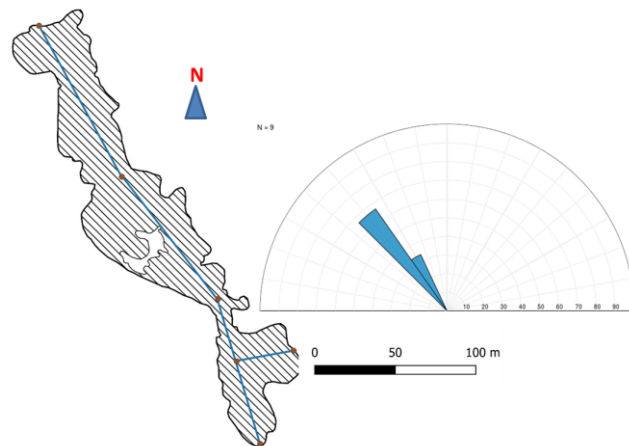


Figure 13 The Rose Diagram of DDM represents the conduit orientation

### *IOI (IOIÔ)*

The IOI Cave is located in the Patos Lagoon Village, in the municipality of Palmeiras, in the state of Bahia, Brazil and is characterized by narrow, sub-parallel cave conduits (Hoop & Prabhakaran, 2018). This cave has only one trend towards NNE-SSW with total 350 m skeleton on that direction. The Rose Diagram also totally represents the actual cave (Figure 14).

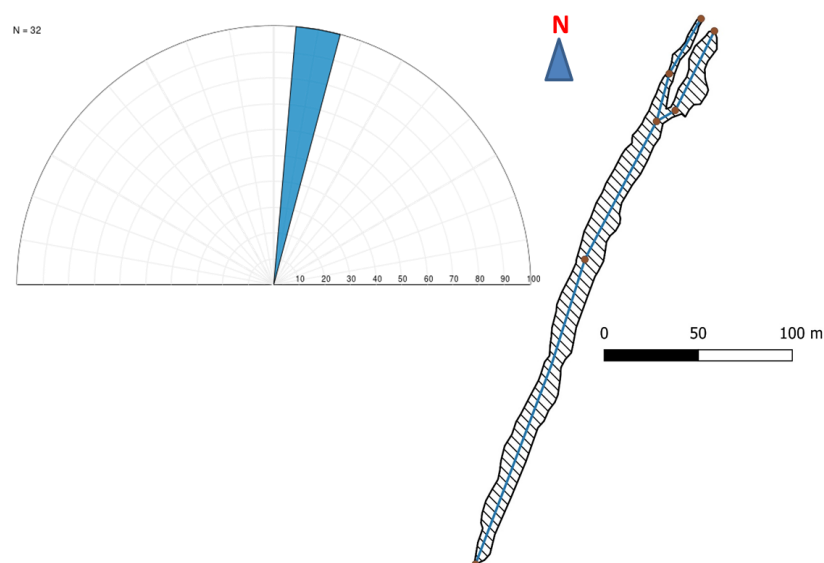


Figure 14 The Rose Diagram of IOIÔ represents the conduit orientation

### ***TOR (Torrinha)***

Torrinha is located in the municipality of Iraquara, in the state of Bahia, Brazil, and it has 12 km long passageways conduits (Hoop & Prabhakaran, 2018). This cave is different from the other caves in terms of dominant conduit orientation; Two main directions can be seen, and they are perpendicular to each other. The first orientation is towards W-E, which is represented as the horizontal tunnels in the 2D map and the NNW-SSE oriented tunnel as the other dominant direction.

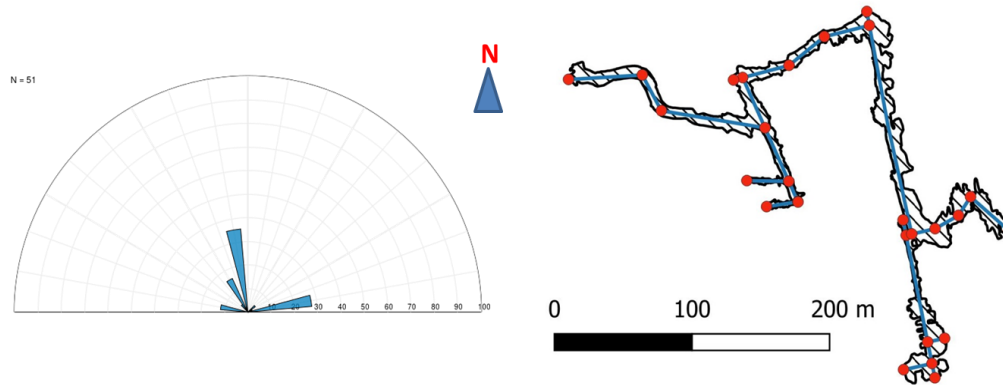


Figure 15 The Rose Diagram of TOR represents the conduit orientation

### ***LAP (Lapinha)***

The Lapinha cave is located in the municipality of Ibiquera, in the state of Bahia, Brazil and it has a series of rectilinear conduits with large internal spaces (Hoop & Prabhakaran, 2018). Generally, the same as Torrinha (TOR) which two main directions of this cave are perpendicular to each other. Above all, the dominant orientation is towards N-S with total length around 240 m of tunnels on that direction and E-W. It is evident because we can see the prevailing direction from the 2D map (Figure 16).

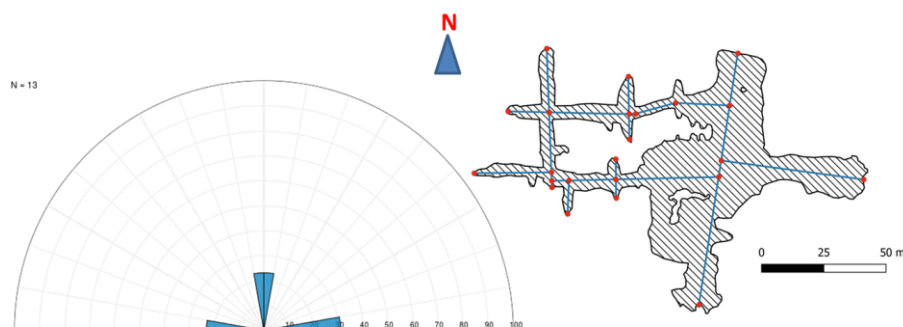


Figure 16 The Rose Diagram of LAP represents the conduit orientation

### ***PAX (Paixão)***

The Paixão Cave is located in the municipality of Andaraí, in the state of Bahia, Brazil. The cave has a series of conduits that are scattered in directions. Based on the Rose Diagram, the NNW-SSE direction is dominant, with in total 200 m length of skeletons in that direction (figure 17).

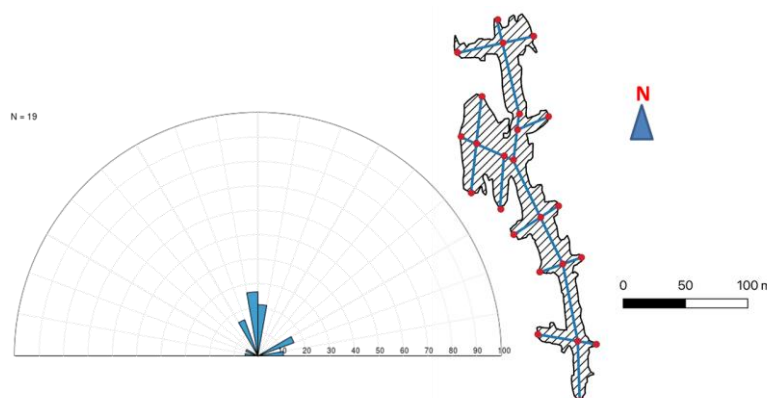


Figure 17 The Rose Diagram of PAX represents the conduit orientation

#### 4.1.1 Conduit Orientation Discussion

The variety of orientation analysis patterns observed in five caves shows the variability that one can encounter when studying karstic systems. Most of the time, preferential orientations relate to particular inception features: tectonic (joints, fractures and faults) or stratigraphic bedding planes: (Filipponi et al., 2009). All of the conduit orientation must be compared to structural data along the caves to be sure the relationship between the structural data to origin of the conduit orientation (see chapter 4.3). In general, the dominant orientation of all five caves is N-S / E-W.

#### 4.2 Tunnel Shape & Aspect Ratio

This process is the approximation to make a scan of the whole body of the tunnel to see the shape pattern. Several slices are made for each of the tunnels. Then, from each of the slices, the aspect ratio is calculated. The aspect ratio of a geometric shape is the ratio of its sizes in different dimensions. Most of the base of the tunnel sometimes not very reliable in point cloud data (since the presence of the sediment, the real base of the tunnel does not appear) (see figure 18). Each shape has a different way to calculate the aspect ratio. All of the tunnel shapes are considered as the ellipses to simplify the analysis. Therefore, the aspect ratio denotes the ratio of the major axis to the minor axis (Figure 19).

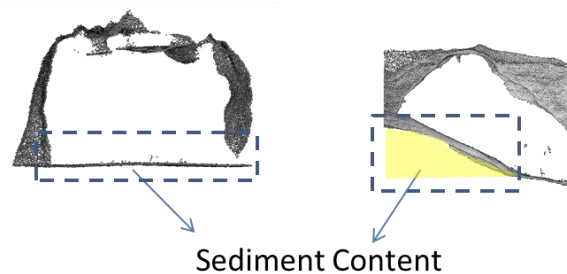


Figure 18 The presence of sediment content that covered the real tunnel base

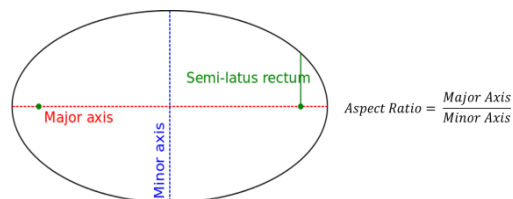


Figure 19 The equation for aspect ratio calculation in ellipse shape

Some error also might happen due to the unclear surface (e.g. slice 5 & 7 of DDM) or some tunnels stacked on top each other (e.g. slice 2 of IOI) which calculate aspect ratio cannot be done.

#### **DDM(Diva de Maura)**

In total, eight slices are made in every 25 meters in this cave. The tunnels in this cave are dominated by Horizontal ellipse shape with aspect ratio value more than 1 (See frequency plot in figure 21). This cave is consist of an extensive body of the tunnel inside with an average of more than 25 m wide. In some cross-sections, the measurement cannot be done due to the unclear surface (see cross-section number 5&7 in figure 20). The highest ratio within all of the caves is also can be seen in cross-section 1 (figure 20).

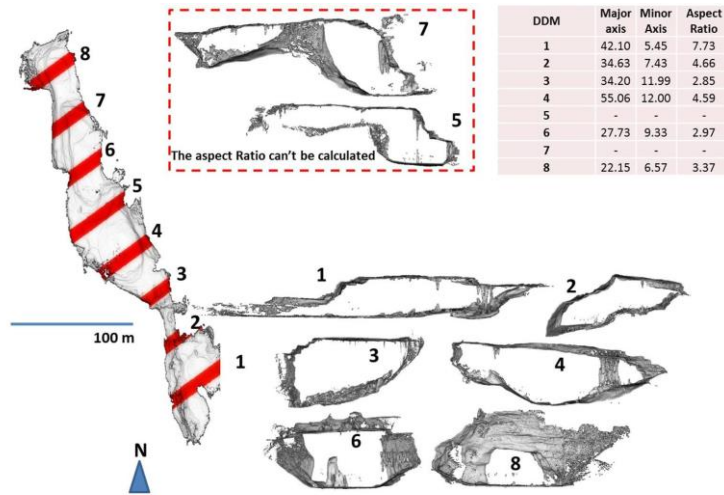


Figure 20 The cross sections & aspect ratio calculations of DDM

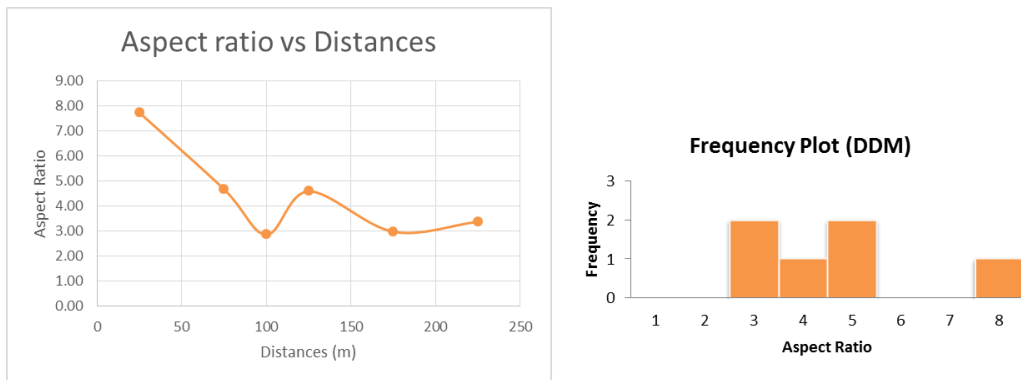


Figure 21 Left : The Aspect Ratio Plot vs Distance (0 m distance starts from the southern part) & Right : The frequency plot of slices of DDM

This wide tunnel shape is caused by the profoundly weathering developed by the underground river which comes from the quartzite recharge area. This cave hypothetically interpreted as an epigene cave that connected to the present (and past) levels of Rio Preto river (Audra et al., 2019). The floor of the cave also covered with dust from disaggregation that can be visible in the point cloud data with a very planar base of the tunnel (see figure 20 slice 1).

IOI (IOI $\hat{O}$ )

IOI	Major axis	Minor Axis	Aspect Ratio
1	17.08	7.85	2.18
2	-	-	-
3	16.33	7.68	2.13
4	15.83	6.30	2.51
5	15.73	4.81	3.27
6	16.28	6.25	2.61
7	13.32	7.29	1.83
8	12.37	7.77	1.59
9	12.35	6.50	1.90
10	12.80	7.47	1.71

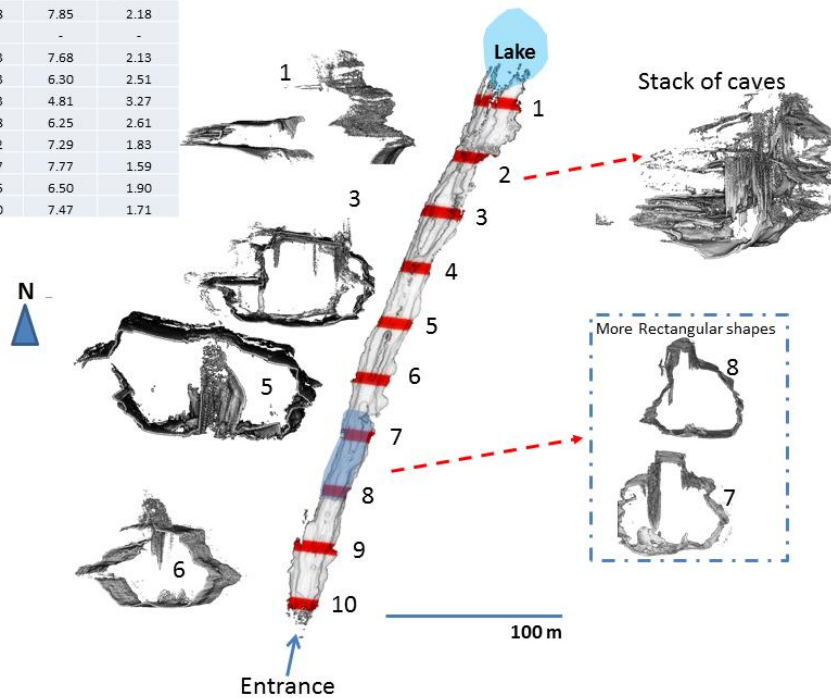


Figure 22 The Cross Sections of IOI & Aspect Ratio Calculation

In general, from 10 slices in each 25 meter, the horizontal ellipses is the dominant shapes of this cave (see frequency plot in figure 23) with the aspect ratio value range 1.59-3.27. However, there is an anomaly in cross-section number 7 & 8 that have more rectangular shapes than the others. Besides that, in cross-section number 2 (figure 22), there is a stack of several tunnels on top of each other, which make the aspect ratio is hard to calculate.

The notch frequently can be seen in some slices. This shape is formed because of the change in the water table. The maximum wide that the tunnel has (the notch) corresponds to the maximal enlargement at the water table (water level A in figure 24). During the time (probably recently, Audra et al., 2019) the groundwater getting overexploited that caused the water level to drop down until several meters (water level B in figure 24). The higher elevation will not get any effect during this process.

Cazarin et al. (2019) said that below the tunnel (it will be clear to see below the lake, see figure 22 for the lake position) there is an ascending conduit (feeders) The presence of feeder is evidence of a hypogenic type of cave since it was formed because of a rising fluid from the bottom part. Away from the feeder, usually the tunnel gradually narrows till a dead-end (Audra et al., 2019), this is also proven that the width of the cave generally decreasing towards slice 10. This is the reason why we find the more rectangular tunnel shape towards the entrance of the tunnel (see the left graph in figure 23).

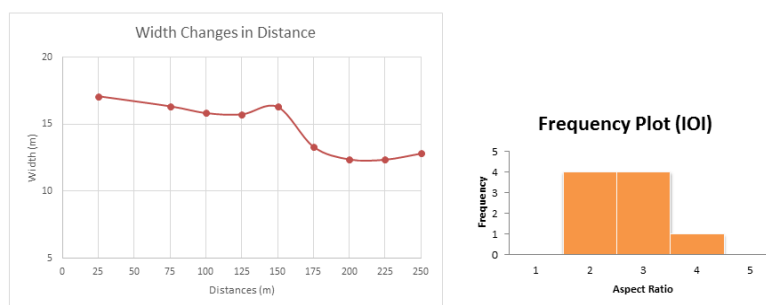


Figure 23 Left : The tunnel width changes of entire slices (0 m distance starts from the lake position), Right : The frequency plot of IOI calculated aspect ratio

This cave is known as a water table maze type of hypogene cave. The water table from the lake mainly controls the development of the cave. It is believed that recently active or probably still. Otherwise, the cave would have been filled by sediments like the other cave, and the morphologies are precisely associated with the present water table (Audra et al., 2019).

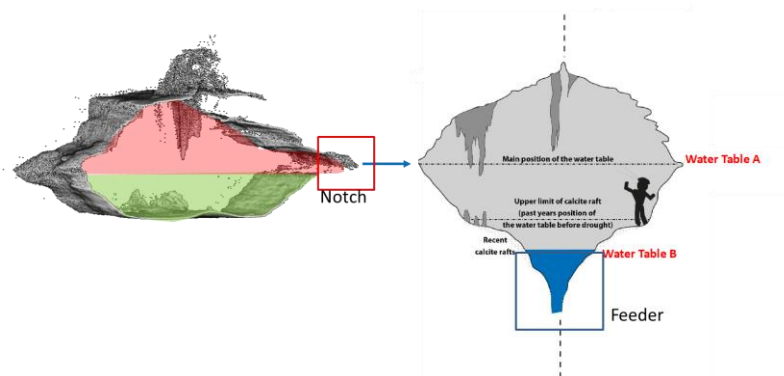


Figure 24 The Illustration of the water table changes effect to the tunnel shape (after Audra et al., 2019)

### TOR (Torrinha)

In this cave, more cross-sections are made to make a clear view of the cave since it has many branches on its body. We divided into two areas in general, eastern part and western part (see figure 25). The west part of the cave is more the meandering part while the east part is more mazes part.

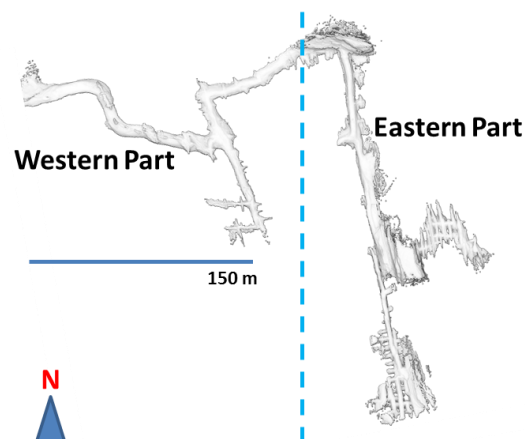


Figure 25 The boundary between eastern part and the western part (dashed line)

In general, the vertical ellipse shape with the aspect ratio below 1 is dominant in the eastern part. Only for cross-section number 2.2 & 2.3 (see figure 26) that look like a horizontal ellipse but if we compared it with cross-section 2.1 which still in the same area (green shaded area, figure 26) it is evident that it is still in vertical ellipse shape. At the green shaded area, the aspect ratio cannot be calculated since there is no clear boundary of the tunnel shape which caused by the less dense of point cloud data.

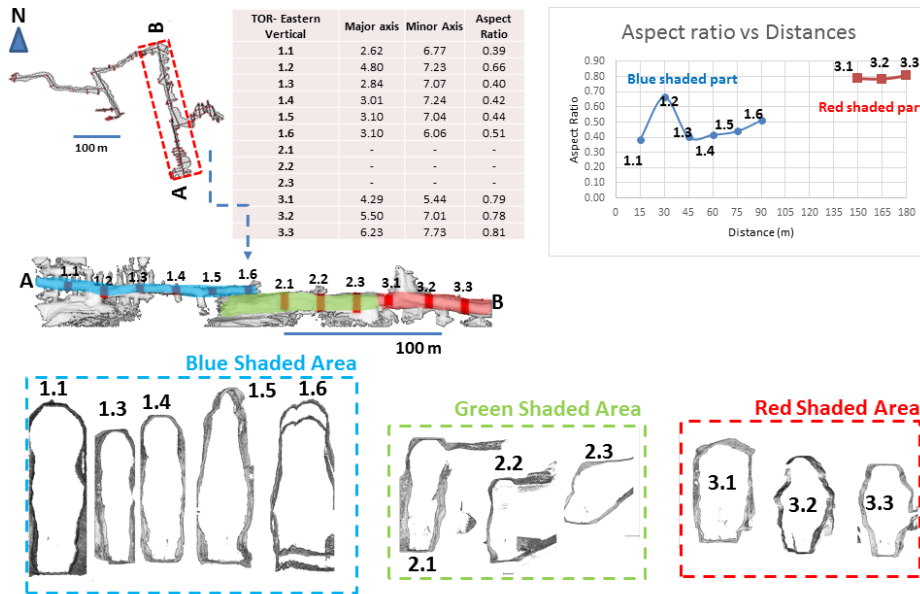


Figure 26 The Details of Cross Sections -TOR (Eastern Vertical Part)

If we take a look into the detail, there are three mazes part in the cave which two are located at the eastern part (Maze 1&2, figure 27) of the cave, and one is at the western part. There is no complete point cloud data for the maze 3, so only the eastern part mazes that processed in this study.

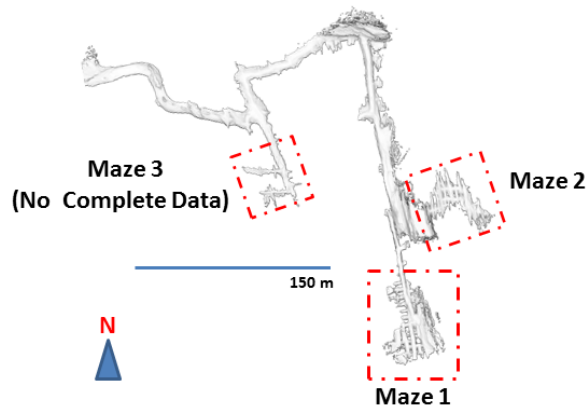


Figure 27 The three mazes part in TOR

In the maze 1 part, it is clear that besides the shape is the same; the aspect ratio also almost the same and it ranges from 0.40-0.75 (figure 28).

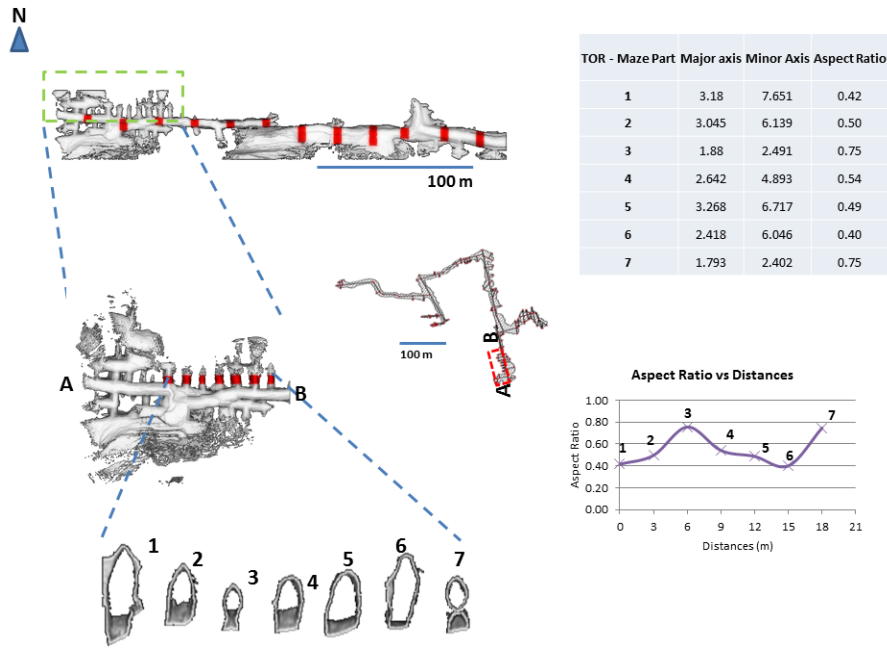


Figure 28 The Details of Cross Sections -The Maze 1 Part

On the other hand, the maze 2 part has a different shape in general compared to the first maze. In this part, mostly, the conduit shapes are more horizontal (see figure 29).

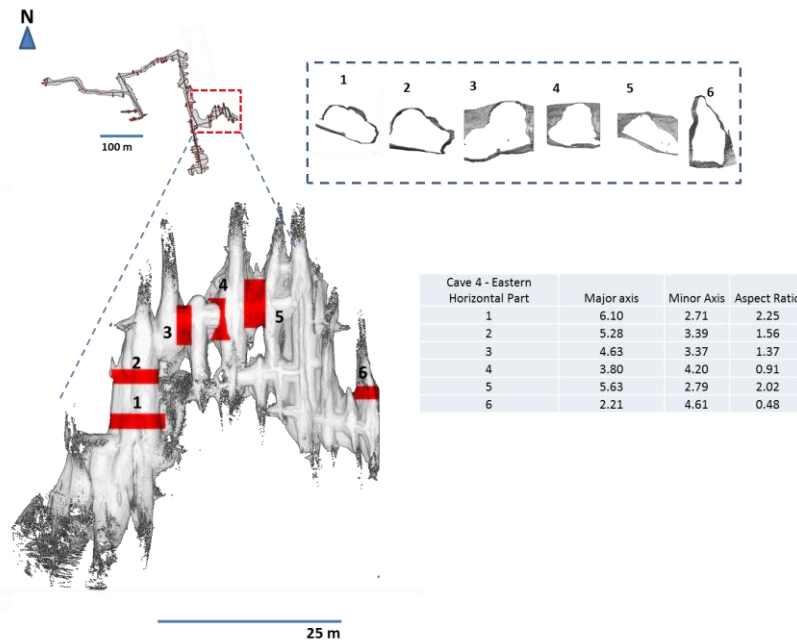


Figure 29 Cross Sections Of The Eastern Horizontal Part of TOR

The things are getting different for the western part which no vertical ellipse shape can be seen anymore. The horizontal ellipses shape has entirely dominated the tunnels with aspect ratio more than 1 (Figure 30 & Table 2).

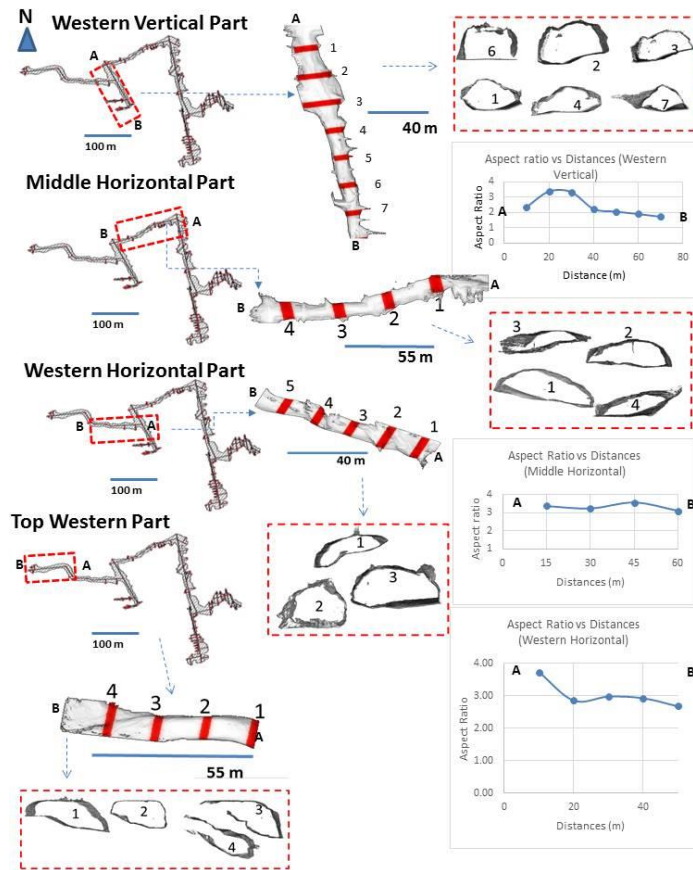


Figure 30 The Details of Cross Section -TOR (Western Part)

Table 2 The Aspect Ratio Calculation of the TOR (western part)

	Major axis	Minor Axis	Aspect Ratio
<b>TOR-Western Vertical</b>			
1	7.92	3.35	2.36
2	11.82	3.49	3.38
3	13	3.88	3.35
4	6.17	2.75	2.24
5	6.12	2.97	2.06
6	5.72	3.01	1.9
7	5.21	3.02	1.72
<b>TOR-Middle Horizontal</b>			
1	9.25	2.74	3.38
2	7.83	2.41	3.25
3	6.32	1.77	3.58
4	9.38	3.01	3.12
<b>TOR-Western Horizontal</b>			
1	8.017	2.147	3.73
2	8.914	3.124	2.85
3	8.306	2.791	2.98
4	11.65	3.98	2.93
5	10.79	4.031	2.68
<b>TOR-Top Western</b>			
1	10.233	2.591	3.95
2	7.802	2.818	2.77
3	-	-	-
4	-	-	-

Based on the shape analysis above, it is clear that the two-part of the cave (western & eastern part) have the different shape of the tunnel (figure 31). The western part of the cave has more horizontal ellipse shape, while the eastern region; (except the maze 2), has more vertical ellipse conduits. The contrast in shapes could be a sign that the two parts of the cave are originated from a different system.

Audra (2019) observed that the west part of the cave is developed by epigenic river system. This condition could produce the shape of the more horizontal conduits since the fluvial system will do the lateral dissolution instead of the vertical direction. Along the meandering part, the passages show a more dominant-conduit pattern with not much mazes. Less deformed zones can cause this condition. However, still, more structural analysis is needed to prove this hypothesis.

However, at the eastern part some extended mazes are present which indicating the different process; probably related to the hypogene origin. Audra (2019) said that the hypogenic system possibly happened first, and the fluvial phase(s) buried them afterwards. This could be the answer to why there are some changes in the shape of the eastern vertical part (figure 26). From the blue shaded to the red shaded part shows that the closer to the meandering part, the more sediment deposited which brought by the fluvial flow. The red shaded part in figure 26 shows the bulky/ more rectangular shapes are indicating the sediment that filling the passage. While going to the Blue shaded part, the narrower conduits can be found, which suggests there are no more fluvial system influences in this part. It possibly an indication that before the fluvial phase comes, the hypogene system created the most of the karst conduits at the eastern part. Then the fluvial period(s) modified some of the forms in that region.

The other exciting part is the different shape between the two eastern mazes (maze 1 & 2, see figure 31). One possibility is caused by the sediment that filled the conduit which brought by the river during the flooding season. Nevertheless, more analysis is needed to see the exact factor that causes a different shape between the two mazes.

This cave is a complete example of both genetic types of karst: hypogene and epigene. The more extended analysis is needed to reveal the process behind the development of the cave system. Even though using the shape analysis can give us some idea of how was the process was, but still, it needs to be proven by other detailed analysis using outcrop data.

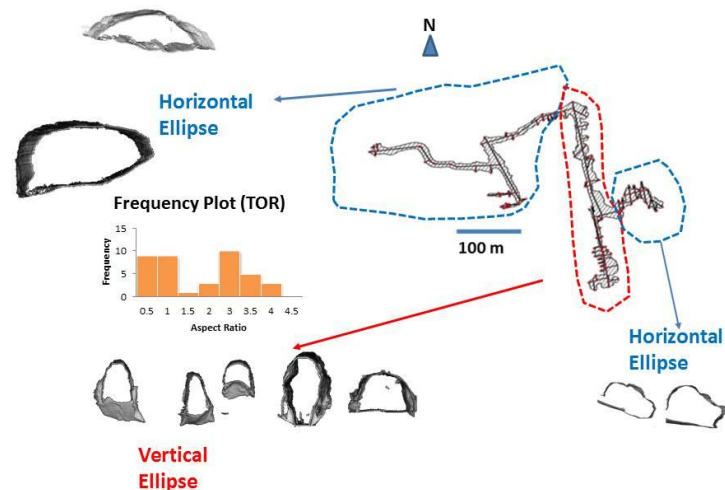


Figure 31 The shape differences between two parts of TOR cave

**LAP (Lapinha)**

This cave is composed of two thin branches of tunnels on the western part and a large body of one tunnel on the eastern side (figure 32). The aspect ratio calculations are done in these two parts of caves.

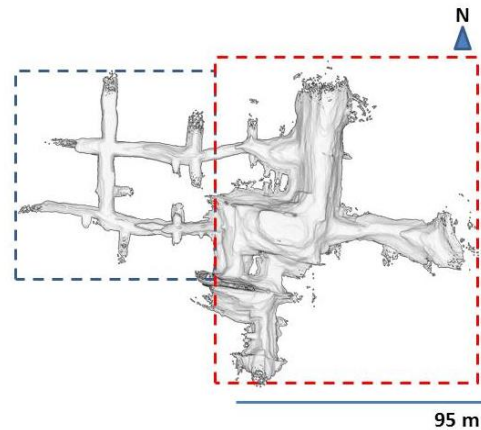


Figure 32 The boundary between thin branches of the tunnel (blue dashed square) & the large body tunnel (red dashed square)

The comparisons of shape & aspect ratio are made at the thin branches. Based on that, it is sure that both of the branches have identical aspect ratio although cross-section number 1 & 3 have different shapes (Figure 33)

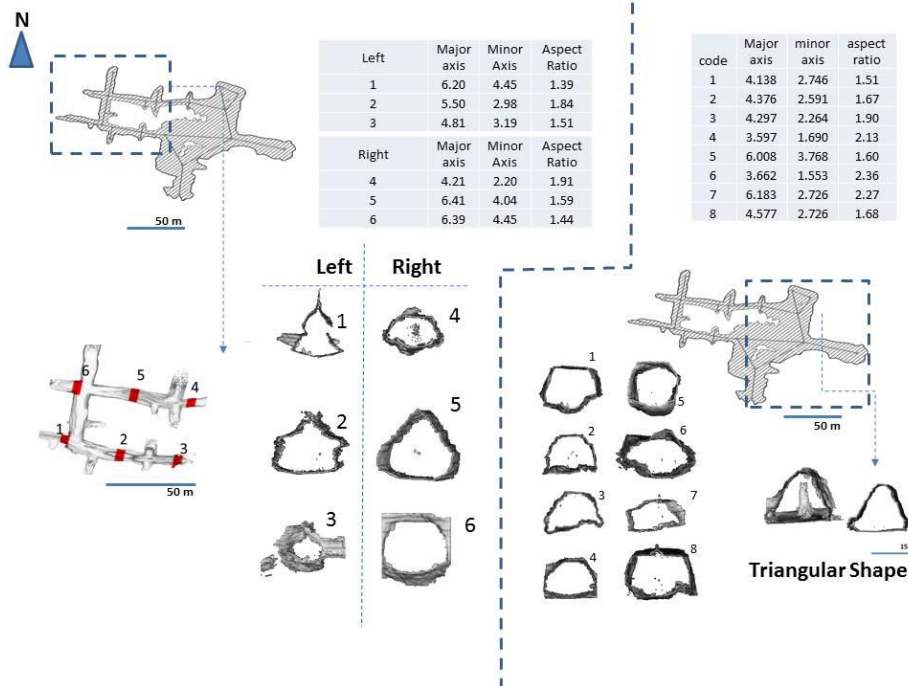


Figure 33 The Shape Comparison between Two Parts - LAP

At the other part of the cave (large body tunnel), the triangular shape can be found (figure 33). Even though it is not clear where is the real base since the flat base of the tunnels usually forms because of the presence of sediment (Audra et al., 2019).

Inside the cave, there is a broad anticline that very short towards E-W but more extensive in N-S direction (Audra et al., 2019). The triangular shape at the eastern part of the cave was formed because of the anticline structure. At several places, the roof is often flat (slice 1, the east part of the cave, figure 33) is located in the more impermeable layers (probably silts) acting perhaps as a seal.

**PAX (Paixão)**

Three different shapes are established in the last cave: Horizontal ellipses, triangular shapes and rectangular-ellipses (Figure 34). The aspect ratio also varied with a range starting from 1.2 until 2.6.

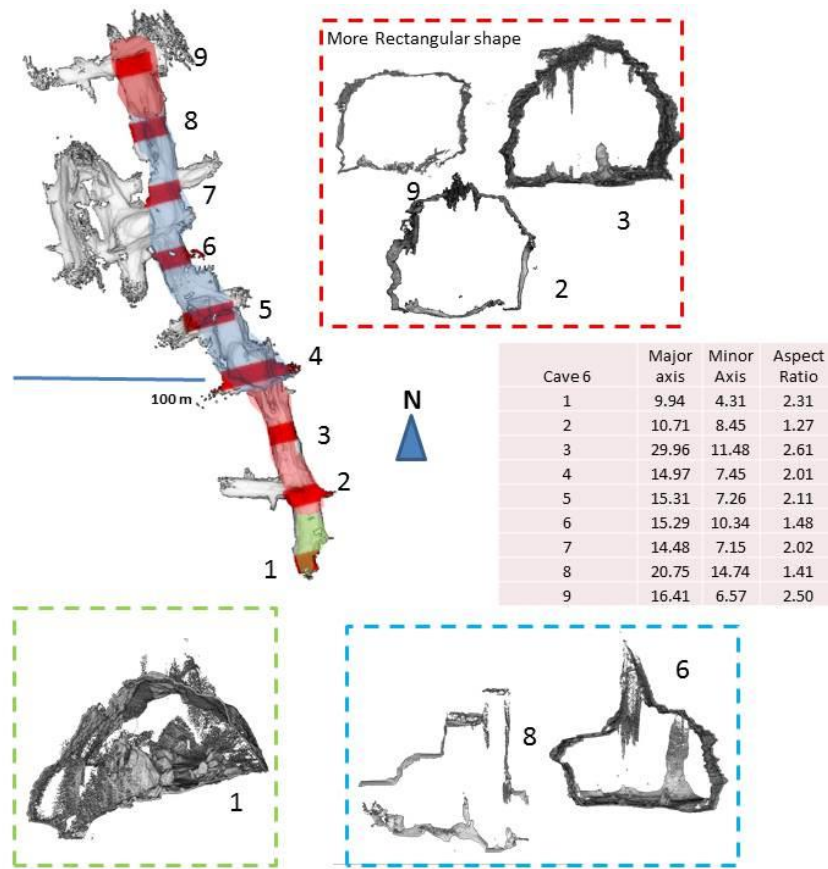


Figure 34 The Cross Sections of PAX: Rectangular-Ellipses Shape (Red Coloured Area), Horizontal Ellipses (Green Coloured Area) and Triangular Shape (Blue Coloured Area)

This cave has the same type as IOIO; Hypogene water table maze (Audra et al., 2019). The difference is this cave has more sediment fills compared to IOIO (see the flat based in almost every slice in figure 34).

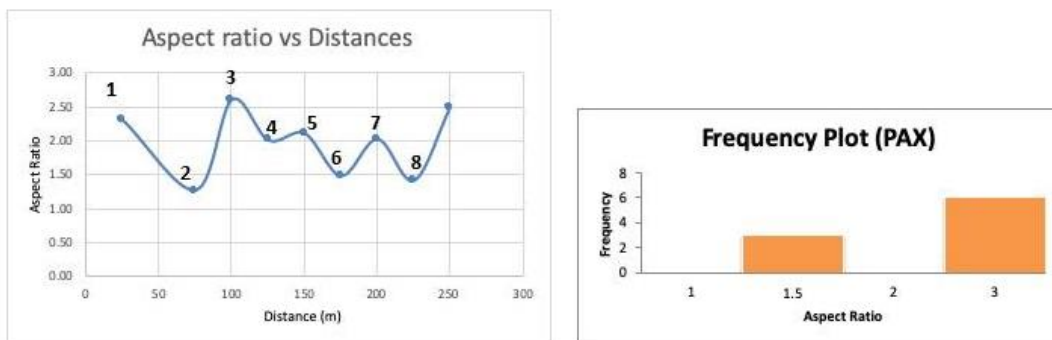


Figure 35 Left : The Aspect Ratio Plot vs & Right : The frequency plot of slices of PAX

#### 4.2.1 Geometry Analysis Discussion

Based on the geometry analysis, it is clear that there are two types of tunnel shapes in general; the horizontal ellipse and the vertical ellipse shape. The horizontal shapes are the most dominant shape compared to the vertical one (figure 36).

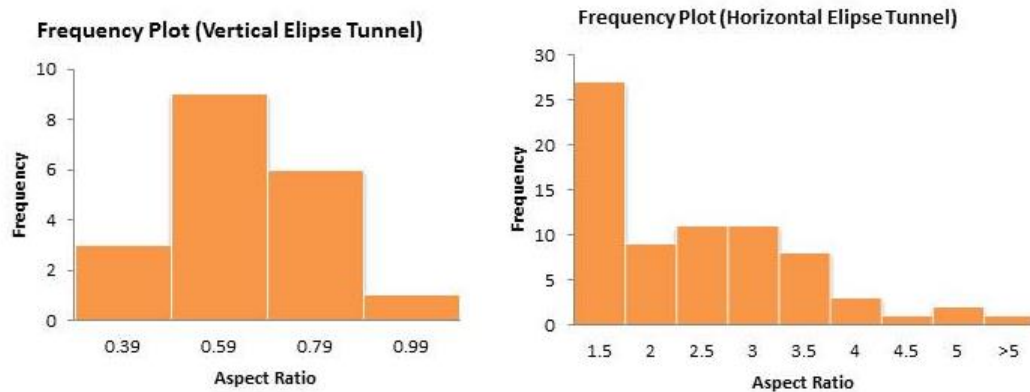


Figure 36 Frequency plots for every tunnel shapes

Several factors could cause the difference in shape. Audra & Palmer (2015) said that the cave systems are controlled by two possible parameters: Passive and boundary condition. The passive parameters consist of lithology type and the tectonic system. While, the boundary condition parameters are the type of recharge, topographic gradient, and base level position. Nevertheless, based on the data that we had in this study, the tectonic and lithology are the parameters that can be proven to control the cave systems.

The lithological factor is essential in karst development. 75% of the earth's surface is covered with sedimentary rocks, and 20% of that consists of limestones or dolomite (Pettijohn, 1975). The karst can occur on carbonates with less purity than 80%, but generally the purer the limestone, the better the development of karst morphology (Jennings, 1971). The different type of lithology can give a different reaction to the dissolution of fluids that will develop the conduits. We can see it from several examples with the stacking shape (see slice 4 in figure 22), the different lithology type will make a particular profile to the conduit with the notch or stacking pattern. The other example is slice one at the eastern part of LAP (see figure 33), the roof is flat. It could be an indication of the presence of the impermeable layer(s) on top of the conduit (e.g., silt/clay) that stop the flow of the fluid and will stop the development of the conduit vertically. The geology structure also played an essential role in the development of the caves. As mentioned above, the shape of the tunnel can preserve some features like the anticline in LAP. Besides that, the geologic structure also can give an idea about the origin of the caves, which will be discussed more in the next chapter (chapter 4.3).

Even though, from the all geometrical analysis above, it could be said that the type of karstification process cannot be directly determined only using the pattern of the shapes. Many tentative questions still need to be answered by the other analysis.

### 4.3 Structural Data Analysis

The structural data that already measured in the fields are fractures and veins (see Appendix 4). Analysis of structural features indicates five main sets specifically: set-1: NNW-SE & set-2: ENE-WSW (DDM), set-3: NNE-SSW (IOI), set 4: N-S & Set 5: W-E (TOR, LAP, PAX).

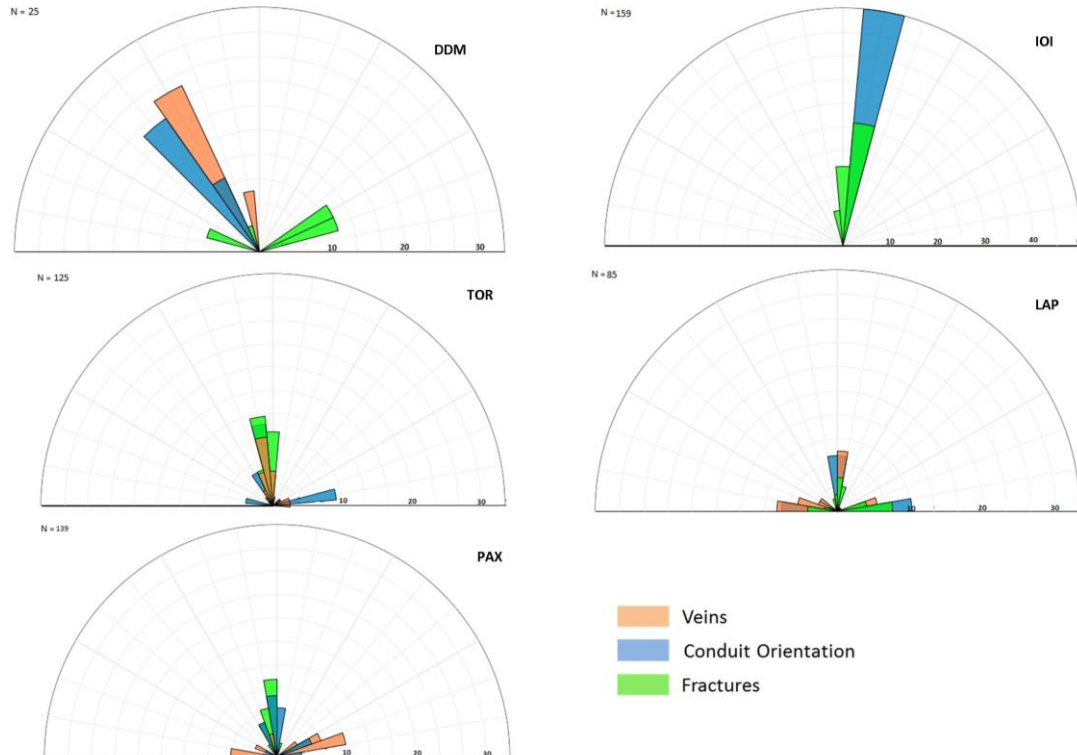


Figure 37 Rose Diagram plot of the structural data and the conduit orientation of all caves

Based on the comparison, both the conduit orientation and the structures data generally show the same trend, which applies to all caves (Figure 37). All of the caves show the primary orientation go to N-S and W-E as the secondary orientation. Therefore, these conditions suggest a geometrical correlation between the fractures and the caves, and that the observed fractures almost certainly acted as conduits for fluid flow. These structures guided the fluid flow and selective dissolution of ascending fluids, which confirms that the conduits are associated with fractures.

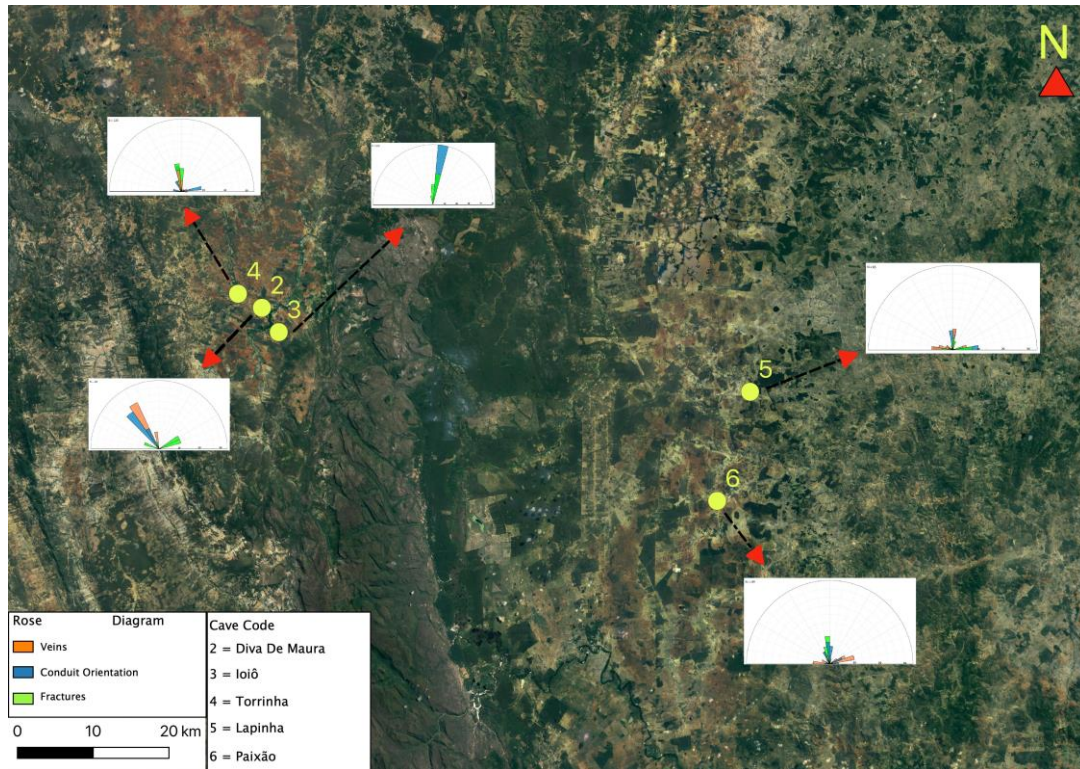


Figure 38 The position map of all the caves + Plotted Rose Diagram

#### 4.4 Stability Analysis

As well to surface and near-surface karstification of carbonate successions, related processes such as the collapse of cave systems may occur during deep burial, resulting in complex reservoir architectures with high spatial heterogeneity (Sayago et al.,2012). The stability analysis allows seeing how each tunnel behaves under several depths of meter into the subsurface. In the software, the material will be failed if the strength factor value is less than 1 at a given point, which indicates that the stress in the material exceeds the material strength. Since the software only specifies the fail for a singular point on the boundary, we decide to put a threshold of 10% failure points of the total points for each tunnel slice as the desired failure depth.

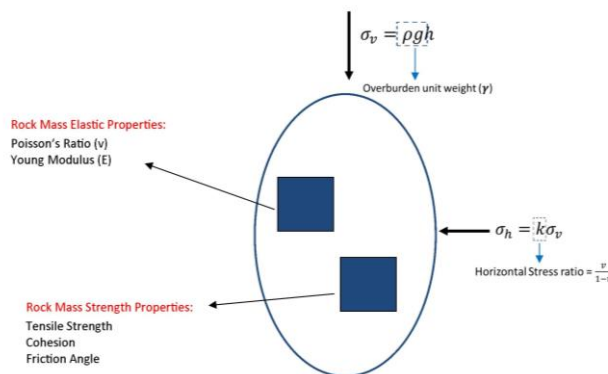


Figure 39 Input parameters for stability analysis

##### Input Parameters

Some parameters are needed as an input for this analysis (figure 39): Rock Mass Stress parameter (Tensile strength, Cohesion & Friction Angle), Rock Mass Elastic (Poisson's Ratio & Young Modulus) and the in-situ field stress (Overburden Unit Weight-Density, Horizontal stress ratio). In this case, the maximum principal stress ( $\sigma_1$ ) is always vertical and guided by the overburden and also the stresses on the horizontal plane are being controlled by Poisson's effect applied by the vertical stress (figure 39). In another way, the tectonic stress was zero.

Every parameter is related one each other, and it will affect the stability of the tunnel. The data used in this experiment are based on the literature. This caused by no availability of any laboratory measurement to the hand specimen of all caves. All of the lithologies that build the cave are assumed as limestone and based on the literature (goodman,1984); there are range numbers of the limestone properties (table 3).

### Modelling Strategy

The idea of the experiment is to see how the effect of shape changes (individual) below particular depth with several parameters applied. Firstly, we used the simple shape as the base case with a total of 11 smooth ellipse shapes are created with a different aspect ratio (Base case) (figure 40). After that, we took several slices that represented the shape for each of the caves (real case) (figure 41). In order to get a representative result, the parameters we used are the middle point for each of the parameter ranges (table 3).

Table 3 Input Data Ranges (Goodman,1989)

ROCK MASS STRENGTH (Goodman,1989)			
	Value Ranges	Preferred Model (mid data)	Unit
Cohesion	6.72 - 23.6	15.16	Mpa
Friction Angle	34.8 - 42	38.4	Degree
Tensile Strength	1.5-4	2.75	Mpa
ROCK MASS ELASTIC (Goodman,1989)			
	Value Ranges	Preferred Model (mid data)	Unit
Poisson's Ratio	0.25-0.3	0.275	-
Young Modulus	47000-71000	59000	Mpa
DENSITY (Goodman,1989)			
	Value Ranges	Preferred Model (mid data)	Unit
Density	1.76-2.5	2.16	g/cm <sup>3</sup>

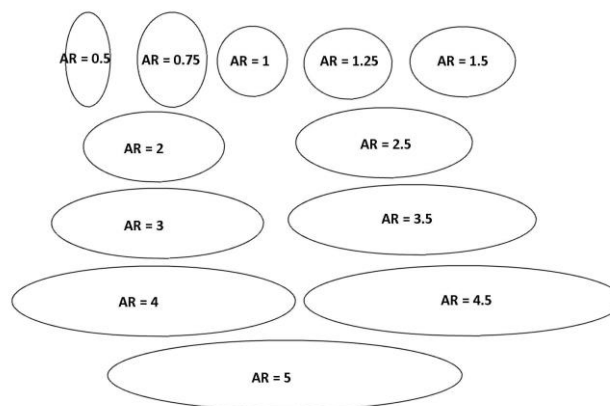


Figure 40 The simple ellipse shapes for base case input

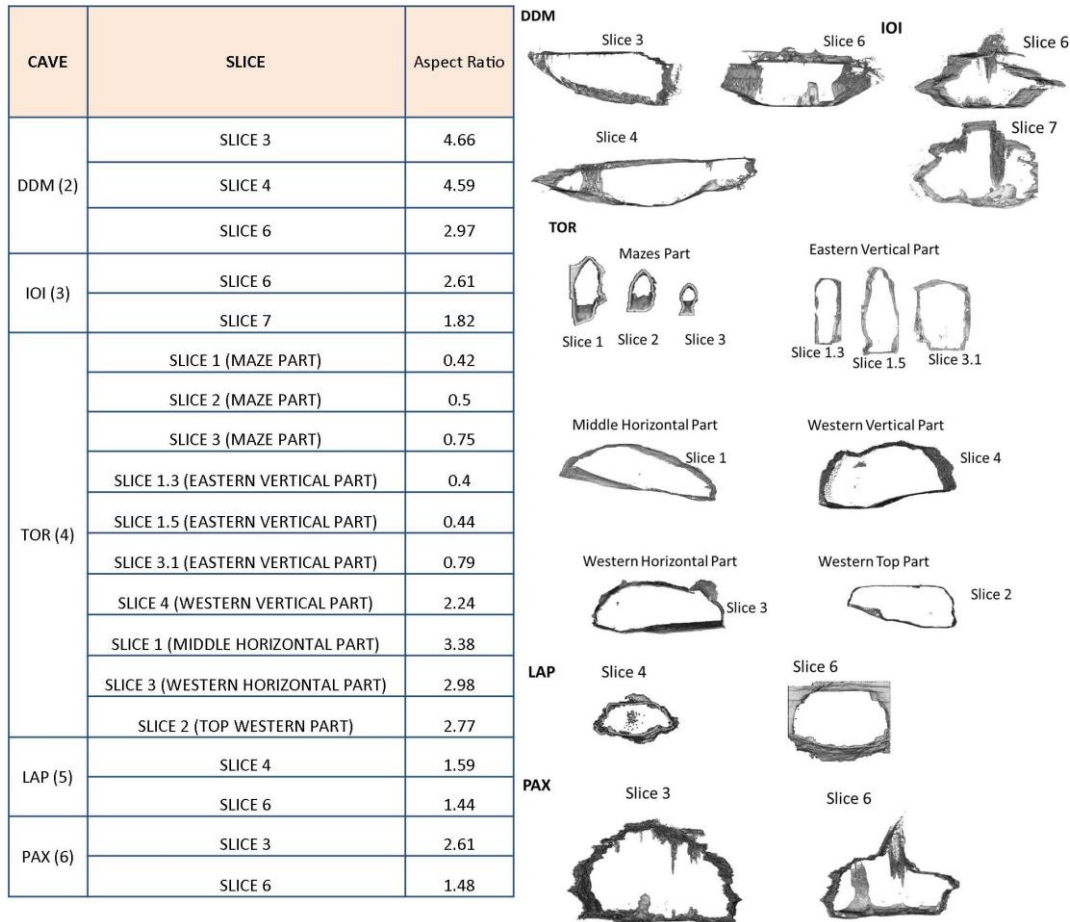


Figure 41 The slices for individual tunnel analysis (Real data)

#### 4.4.1 Base Case

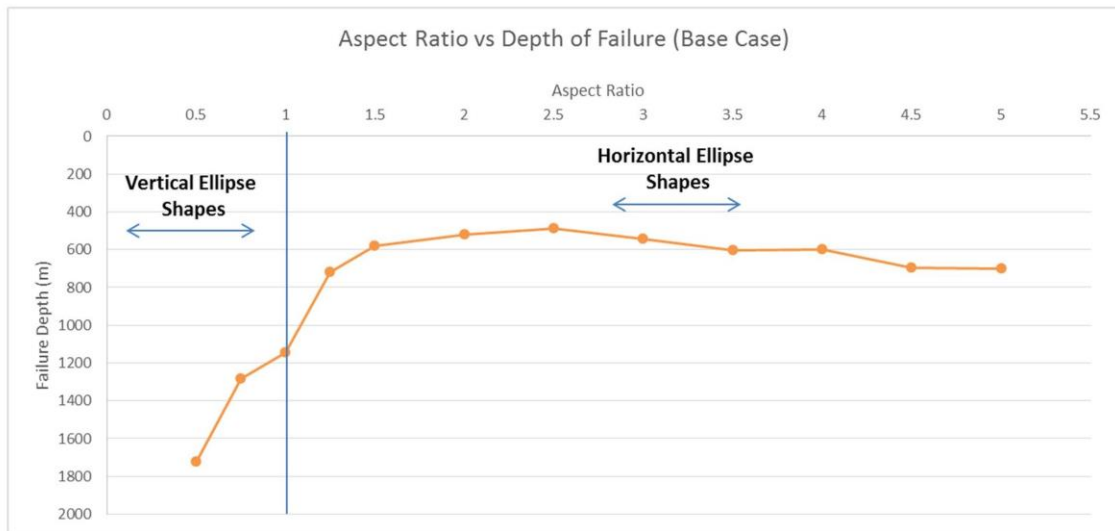


Figure 42 Aspect Ratio vs Depth of Failure Plot (Base Case)

Based on the experiment (using simple shapes), it shows during this condition and applied parameter: all of the tunnels are failed at the shallow depth (in average 800 m) (see figure 42 & table 4). **The numbers show that all of the vertical ellipse shapes are more stable than the horizontal ellipse.** The failure depths are changing significantly for 0.5-1.25 aspect ratio region while it is getting less fluctuated in 1.5-5 aspect ratio region.

Table 4 Failure Depth for The Base Case

Aspect Ratio	Failure Depth (m)
0.5	1722
0.75	1282
1	1146
1.25	718
1.5	582
2	520
2.5	487
3	543
3.5	606
4	600
4.5	697
5	700

#### 4.4.2 Real Case (Individual Tunnel)

Using the Slices from the real caves, **showed that all of the tunnels are geomechanically not stable if we put it into greater depth. (<2 km).** The slices from TOR are the most stable one with the average of the failure depth at 500 m. Instead, the slices from IOI are the most unstable among the others with the average of the failure depth at 150 m. (Figure 43 & Table 5).

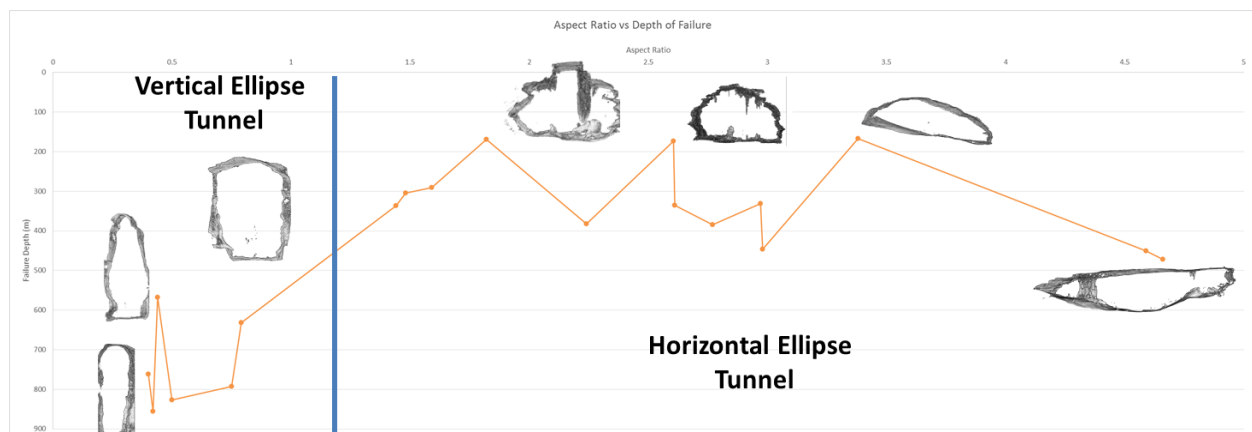


Figure 43 Aspect Ratio vs Depth of Failure Plot (Real Case)

Table 5 Failure Depth for The Real Case (Individual Tunnel)

CAVE	SLICE	ASPECT RATIO	FAILURE DEPTH (m)
TOR	SLICE 1.3 (EASTERN VERTICAL PART)	0.40	762
TOR	SLICE 1 (MAZE PART)	0.42	856
TOR	SLICE 1.5 (EASTERN VERTICAL PART)	0.44	568
TOR	SLICE 2 (MAZE PART)	0.50	827
TOR	SLICE 3 (MAZE PART)	0.75	793
TOR	SLICE 3.1 (EASTERN VERTICAL PART)	0.79	632
LAP	SLICE 6	1.44	337
PAX	SLICE 6	1.48	304
LAP	SLICE 4	1.59	291
IOI	SLICE 7	1.82	169
TOR	SLICE 4 (WESTERN VERTICAL PART)	2.24	382
IOI	SLICE 6	2.61	173
PAX	SLICE 3	2.61	335
TOR	SLICE 2 (TOP WESTERN PART)	2.77	384
DDM	SLICE 6	2.97	331
TOR	SLICE 3 (WESTERN HORIZONTAL PART)	2.98	446
TOR	SLICE 1 (MIDDLE HORIZONTAL PART)	3.38	167
DDM	SLICE 4	4.59	451
DDM	SLICE 3	4.66	472

The fluctuated results in the real case (individual tunnel) showed that the real shape of all tunnels is not smooth enough as an ellipse. Compared to the base case, the real slices are more unstable to the base case slice (figure 44). The comparison concludes that the roughness shape will make the tunnel less stable because the corners with sharp edges will have very high-stress concentration.

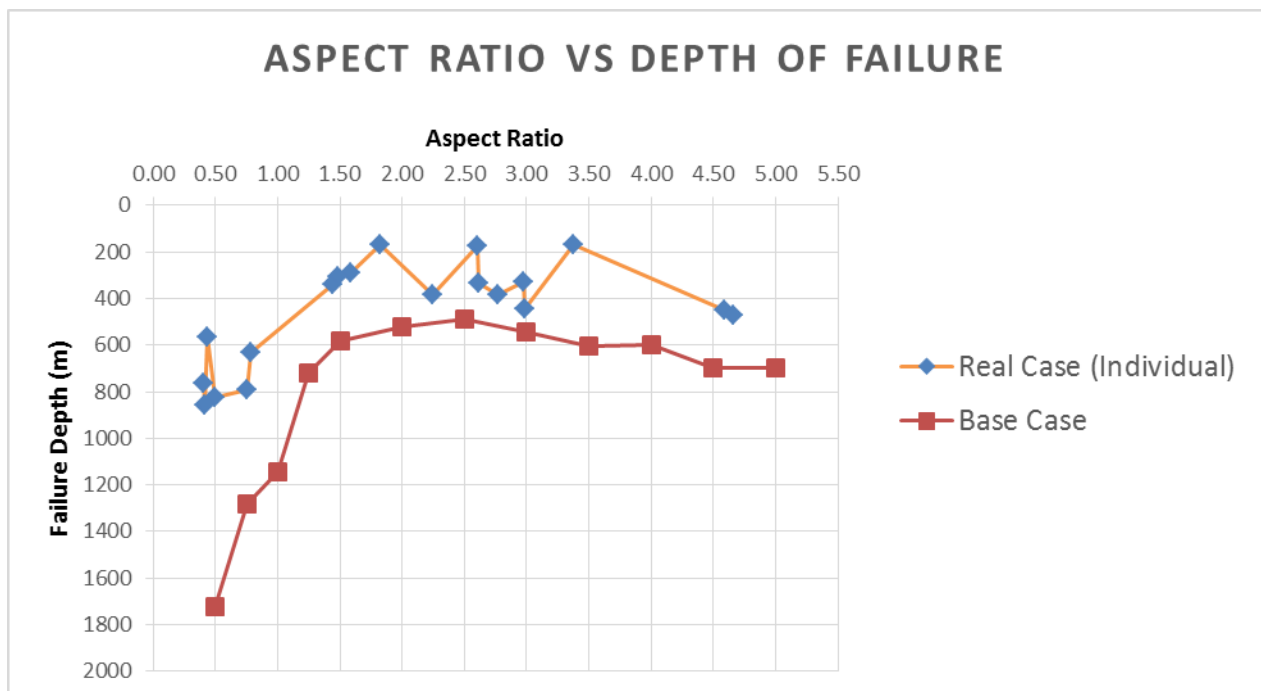


Figure 44 Failure Depth comparison (Base Case vs Real Case (Individual))



The detailed result for each of the case from each of the tunnels is represented in table 7 & figure 46.

Table 7 Failure depth in respect to rock mass strength changes

CAVE	SLICE	ASPECT RATIO	FAILURE DEPTH (m)		
			LOW	REAL	HIGH
TOR	SLICE 1.3 (EASTERN VERTICAL PART)	0.4	315	762	1296
TOR	SLICE 1 (MAZE PART)	0.42	353	856	1444
TOR	SLICE 1.5 (EASTERN VERTICAL PART)	0.44	234	568	958
TOR	SLICE 2 (MAZE PART)	0.5	314	827	1284
TOR	SLICE 3 (MAZE PART)	0.75	293	793	1096
TOR	SLICE 3.1 (EASTERN VERTICAL PART)	0.79	263	632	1063
LAP	SLICE 6	1.44	134	337	538
PAX	SLICE 6	1.48	128	304	511
LAP	SLICE 4	1.59	121	291	490
IOI	SLICE 7	1.82	75	169	279
TOR	SLICE 4 (WESTERN VERTICAL PART)	2.24	158	382	638
IOI	SLICE 6	2.61	72	173	291
PAX	SLICE 3	2.61	138	335	568
TOR	SLICE 2 (TOP WESTERN PART)	2.77	161	384	646
DDM	SLICE 6	2.97	218	331	556
TOR	SLICE 3 (WESTERN HORIZONTAL PART)	2.98	185	446	750
TOR	SLICE 1 (MIDDLE HORIZONTAL PART)	3.38	72	167	278
DDM	SLICE 4	4.59	193	451	768
DDM	SLICE 3	4.66	201	472	820

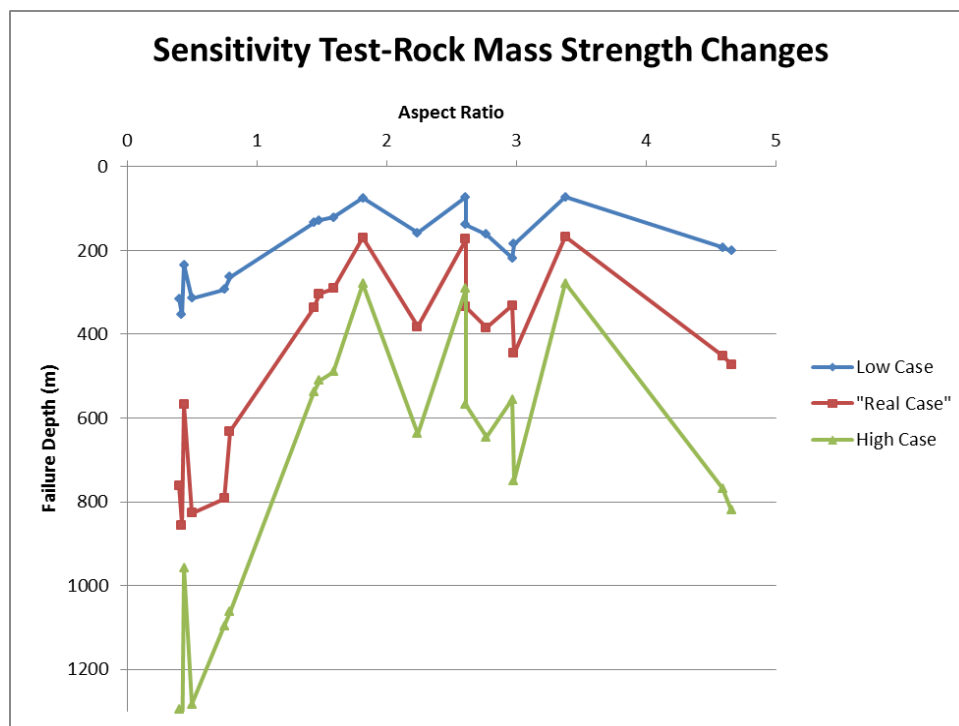


Figure 46 Sensitivity Test Results (Rock Mass Strength Changes)

### Rock Mass Elastic Changes

This group is related to the stiffness of the materials. Two parameters changed during the analysis: Young modulus and Poisson's ratio. Young Modulus (E) represents the resistance of a material to elastic (recoverable) deformation under load. A stiff material has a high Young's modulus and its shape only slightly under elastic loads. On the other side, flexible material has a low Young's modulus and changes its shape considerably. Poisson's ratio is the ratio of transverse contraction strain to longitudinal extension strain in the direction of the stretching force. In other words, the Poisson ratio is the fraction of expansion divided by the fraction of compression, which will define how flexible material is. The higher the Poisson's Ratio of a material, the more flexible it will be.

Therefore, during this group parameter change, we also change the horizontal stress ratio for each of the Poisson's ratio value. Table 8 shows all of the input parameters for this analysis. The low case is the condition when the rock is less stiff compared to the high case.

Table 8 The Input of Rock Mass Elastic Changes

	$\nu$	E (Mpa)	k( $\nu$ dependent)
<b>low case</b>	0.3	47000	0.43
<b>Real Case</b>	0.275	59000	0.38
<b>high case</b>	0.25	71000	0.33

The results in Table 9 shows that there is only a slightly stability changes among all of the tunnels that indicate the elastic parameter (Poisson's Ratio & Young Modulus) are not play an important role in respect to failure depth of the tunnel.

Table 9 Failure Depth in Respect to Rock Mass Elastic Changes

CAVE	SLICE	ASPECT RATIO	FAILURE DEPTH (m)		
			LOW	REAL	HIGH
TOR	SLICE 1.3 (EASTERN VERTICAL PART)	0.4	765	762	759
TOR	SLICE 1 (MAZE PART)	0.42	858	856	854
TOR	SLICE 1.5 (EASTERN VERTICAL PART)	0.44	571	568	566
TOR	SLICE 2 (MAZE PART)	0.5	829	827	824
TOR	SLICE 3 (MAZE PART)	0.75	796	793	790
TOR	SLICE 3.1 (EASTERN VERTICAL PART)	0.79	635	632	631
LAP	SLICE 6	1.44	339	337	332
PAX	SLICE 6	1.48	307	304	300
LAP	SLICE 4	1.59	295	291	288
IOI	SLICE 7	1.82	171	169	167
TOR	SLICE 4 (WESTERN VERTICAL PART)	2.24	385	382	380
IOI	SLICE 6	2.61	175	173	171
PAX	SLICE 3	2.61	337	335	334
TOR	SLICE 2 (TOP WESTERN PART)	2.77	388	384	381
DDM	SLICE 6	2.97	333	331	330
TOR	SLICE 3 (WESTERN HORIZONTAL PART)	2.98	448	446	440
TOR	SLICE 1 (MIDDLE HORIZONTAL PART)	3.38	170	167	163
DDM	SLICE 4	4.59	512	509	504
DDM	SLICE 3	4.66	649	639	633

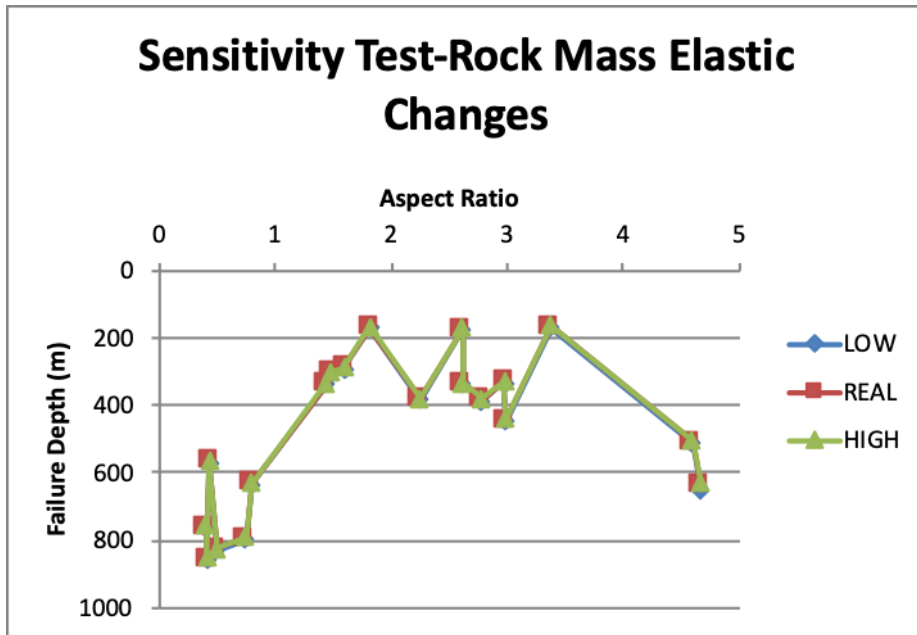


Figure 47 Sensitivity Test Results (Rock Mass Elastic Changes)

### Density Changes

Vertical stress is one of the parameters that can be adjusted in the software. Over any significant horizontal surface within the ground, the average vertical stress must equilibrate the downward force of the weight of the overlying rock. In another way, It is dependent on the density of the materials and can be expressed as :

$$\sigma_v = \gamma h$$

Which  $\gamma$  is a unit weight that equal to :

$$\gamma = \rho g h$$

We assume that every tunnel has the same value of gravity, and the same lithology (Limestone). Hence, in this case, it is fair to say that we compare the failure depth for the density changes. The value of density is taken from the literature (Goodman,1989), and it is ranged as follow :

Table 10 The input of density changes

	Density (g/cm <sup>3</sup> )
low case	1.76
Real case	2.16
high case	2.5

The failure depth shows the relation that the higher the density, the unstable the tunnel is. See table 11 for the detailed failure depth for each of the case.

Table 11 Failure Depth in Respect to Density Changes

CAVE	SLICE	ASPECT RATIO	FAILURE DEPTH (m)		
			LOW	REAL	HIGH
TOR	SLICE 1.3 (EASTERN VERTICAL PART)	0.4	938	762	660
TOR	SLICE 1 (MAZE PART)	0.42	1053	856	740
TOR	SLICE 1.5 (EASTERN VERTICAL PART)	0.44	698	568	491
TOR	SLICE 2 (MAZE PART)	0.5	936	827	658
TOR	SLICE 3 (MAZE PART)	0.75	891	793	615
TOR	SLICE 3.1 (EASTERN VERTICAL PART)	0.79	777	632	547
LAP	SLICE 6	1.44	393	337	278
PAX	SLICE 6	1.48	550	304	264
LAP	SLICE 4	1.59	357	291	252
IOI	SLICE 7	1.82	206	169	147
TOR	SLICE 4 (WESTERN VERTICAL PART)	2.24	455	382	321
IOI	SLICE 6	2.61	213	173	150
PAX	SLICE 3	2.61	412	335	290
TOR	SLICE 2 (TOP WESTERN PART)	2.77	472	384	333
DDM	SLICE 6	2.97	405	331	284
TOR	SLICE 3 (WESTERN HORIZONTAL PART)	2.98	548	446	386
TOR	SLICE 1 (MIDDLE HORIZONTAL PART)	3.38	204	167	145
DDM	SLICE 4	4.59	747	451	404
DDM	SLICE 3	4.66	780	472	410

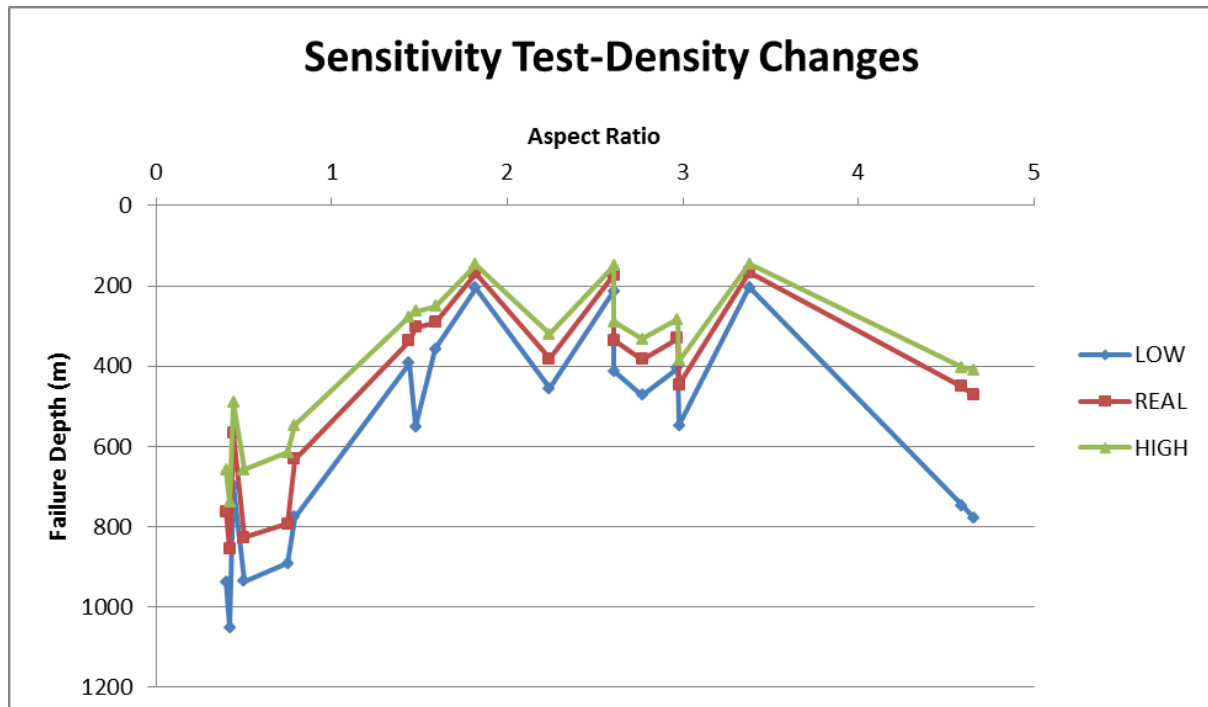


Figure 48 Sensitivity Test Results (Density Changes)

### Group Parameter Changes Comparison

From all of the experiment of parameter changes, it is clear that Rock mass strength changes are playing the main role in terms of tunnel stability (figure 49). The detailed tornado plots of all slices can be seen in appendix 6.

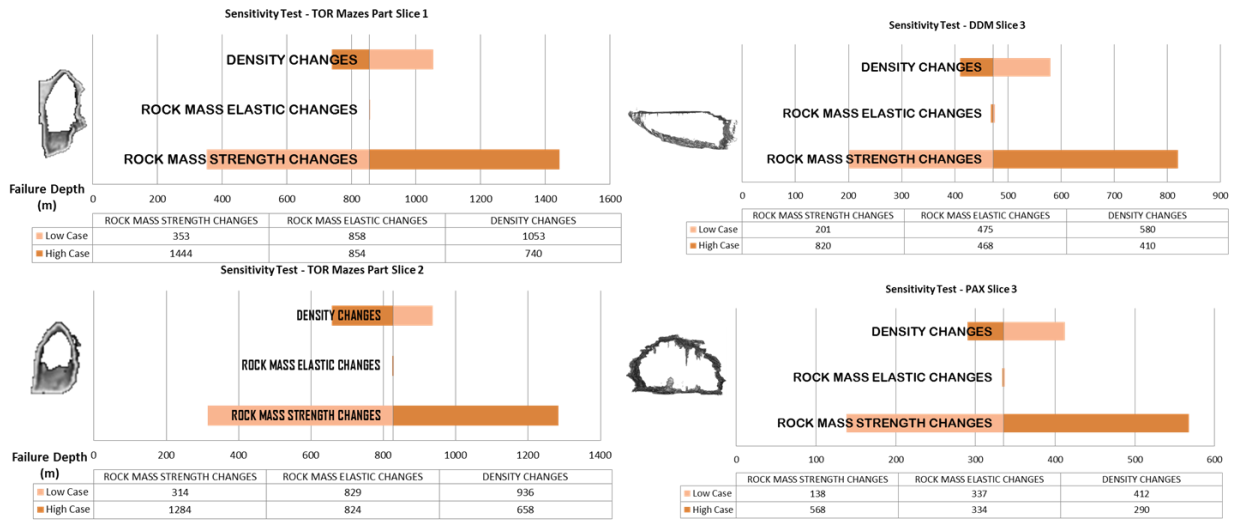


Figure 49 The sensitivity tornado plot for all of the parameter changes

#### 4.5.2 Sensitivity Test-Multiple Tunnels analysis

On the previous chapter, the stability analysis is done on the single tunnel. In Torrinha cave (TOR) we have the maze that has multiple tunnels inside of it. Afterward, the other analysis is done with the same parameter added but with multiple tunnels in one place. During this analysis, we studied the two and three tunnels together with slice 1, slice 2, and slice 3 from TOR maze part as the sample data.

#### Two Tunnels Analysis

The two tunnels (slice 1 & slice 2) are arranged with the same spacing (6 m : Measured from the middle point of one tunnel to the middle point of the other tunnel) as the real condition measurement. The output is different from the single tunnel analysis in both of the tunnel slices (see figure 51 & Table 12).

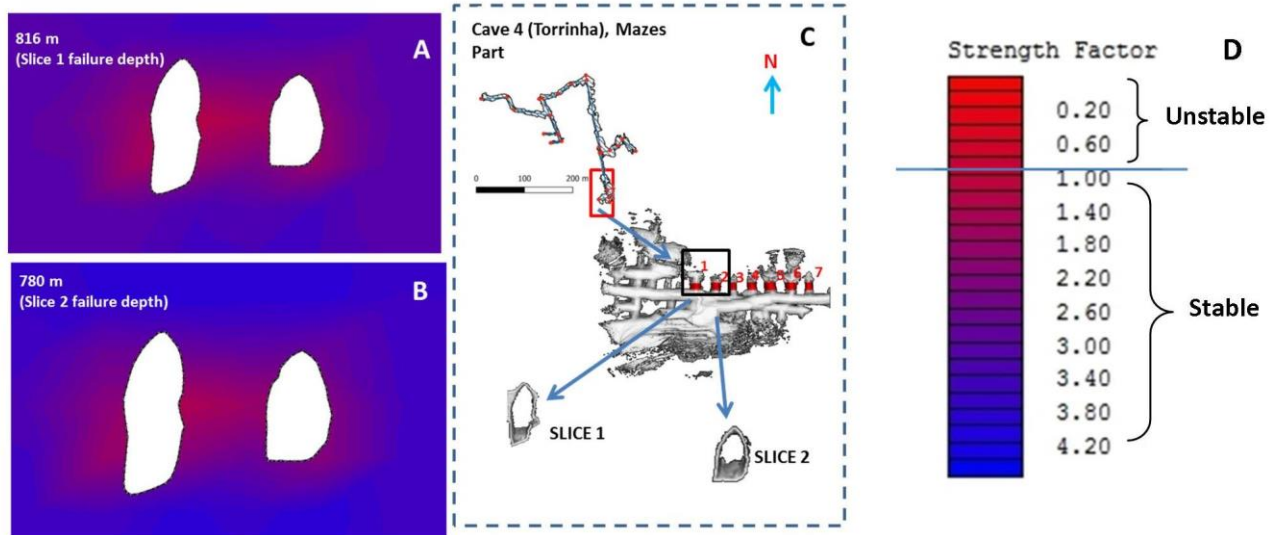


Figure 50 (A&B) The failure contour for the two tunnels analysis, (c): The position of the slices on the map, (d) The scale bar legends (the red colour bar represents the failure and the blue represents the non failure area)

Table 12 Individual tunnel analysis & two tunnels analysis results

Individual Tunnel Analysis	CAVE	SLICE	ASPECT RATIO	FAILURE DEPTH (m)
	TOR	SLICE 1 (MAZE PART)	0.42	856
		SLICE 2 (MAZE PART)	0.50	827
Two Tunnels Analysis	CAVE	SLICE	ASPECT RATIO	FAILURE DEPTH (m)
	TOR	SLICE 1 (MAZE PART)	0.42	816
		SLICE 2 (MAZE PART)	0.50	780

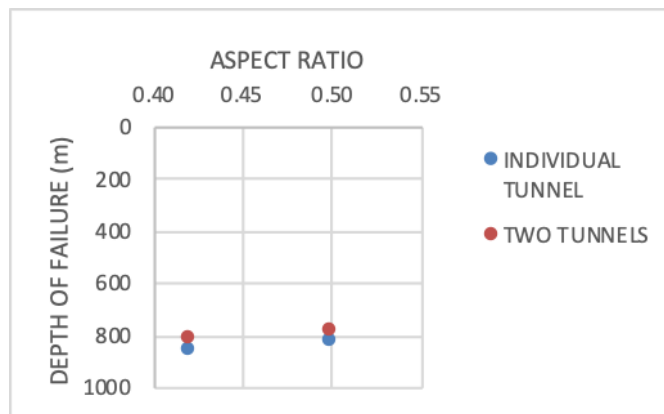


Figure 51 Individual Tunnel analysis vs Two Tunnels analysis Failure Depth Plot

From table 12 & Figure 51 shows that the stability of both tunnel slices are decreasing compared to the individual tunnel analysis.

**Three Tunnels Analysis**

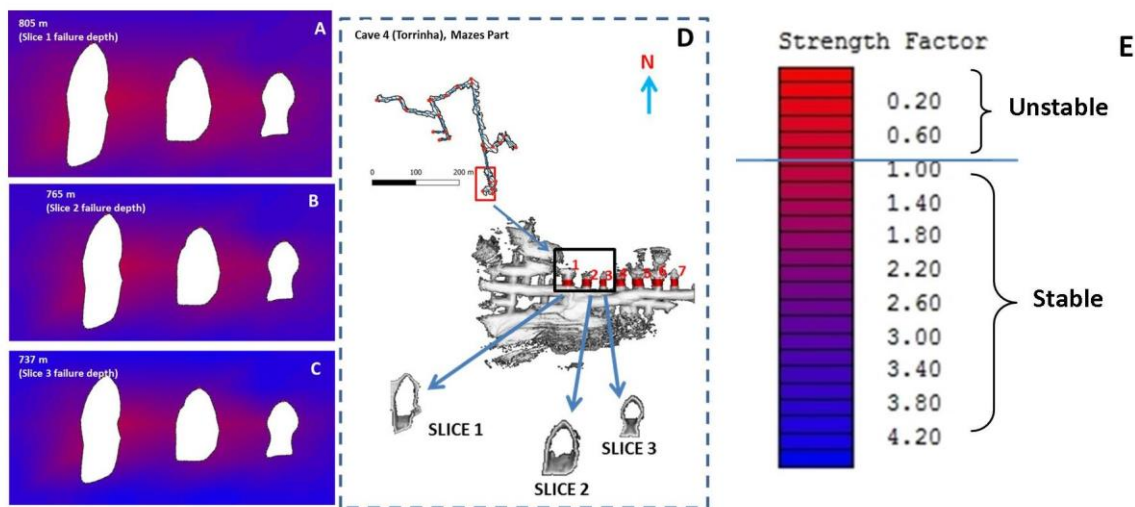


Figure 52 (A,B&C) The Failure Contour for The Two Tunnels Analysis, (D): The Position of the slices on the map, (E) The Scale Bar Legends (The Red Colour Bar Represents The Failure and The Blue Represents The Non Failure Area)

Slice 1, Slice 2 and slice 3 of TOR (Maze Part) maze part are placed together with the same spacing with the real condition in between. Same as the two tunnels analysis, it is noticeable that the tunnels become unstable. (see table 13 & Figure 53 ).

Table 13 Individual tunnel analysis & two tunnels analysis results

individual tunnel	CAVE	SLICE	ASPECT RATIO	FAILURE DEPTH (m)
	TOR (4)	SLICE 1 (MAZE PART)	0.42	856
		SLICE 2 (MAZE PART)	0.50	827
		SLICE 3 (MAZE PART)	0.75	793
3 tunnels	CAVE	SLICE	ASPECT RATIO	FAILURE DEPTH
	TOR (4)	SLICE 1 (MAZE PART)	0.42	805
		SLICE 2 (MAZE PART)	0.50	765
		SLICE 3 (MAZE PART)	0.75	737

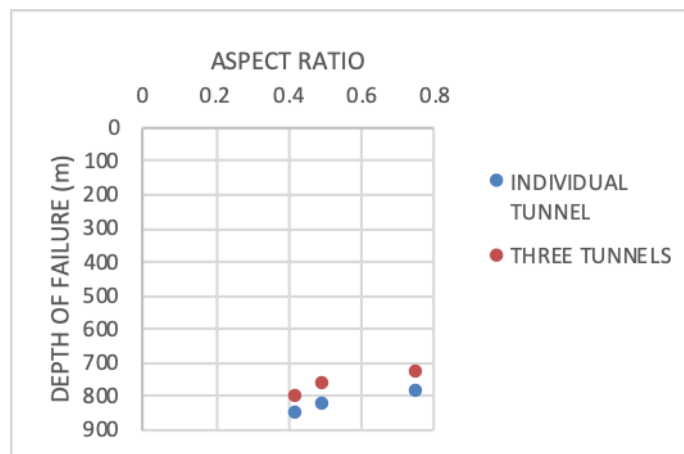


Figure 53 Individual Tunnel analysis vs Two Tunnels analysis Failure Depth Plot

Generally, the multiple tunnel analysis shows that the stability of all tunnels are dependent on the quantity of the tunnels in the system. The more tunnels in the system, the more unstable it will be.

#### 4.5.3 Sensitivity Test – Spacing Changes

For this sensitivity test, we picked the 3 slices from TOR Maze part (slice 1,2&3) all together into the experiment (Table 14 & Figure 54).

Table 14 Sensitivity Test -Spacing Changes Results

CAVE	SLICE	ASPECT RATIO	SPACING	FAILURE DEPTH (m)
TOR	SLICE 1	0.42	6 m (Real Case)	805
	SLICE 2	0.50		695
	SLICE 3	0.75		712
	SLICE 1	0.42	9 m	827
	SLICE 2	0.50		800
	SLICE 3	0.75		761
	SLICE 1	0.42	18 m	844
	SLICE 2	0.50		820
	SLICE 3	0.75		786
	SLICE 1	0.42	25 m	850
	SLICE 2	0.50		831
	SLICE 3	0.75		795
	SLICE 1	0.42	30 m	851
	SLICE 2	0.50		832
	SLICE 3	0.75		796
	SLICE 1	0.42	35 m	852
	SLICE 2	0.50		833
	SLICE 3	0.75		797
	SLICE 1	0.42	40 m	852
	SLICE 2	0.50		833
	SLICE 3	0.75		797
	SLICE 1	0.42	45 m	852
	SLICE 2	0.50		833
	SLICE 3	0.75		797

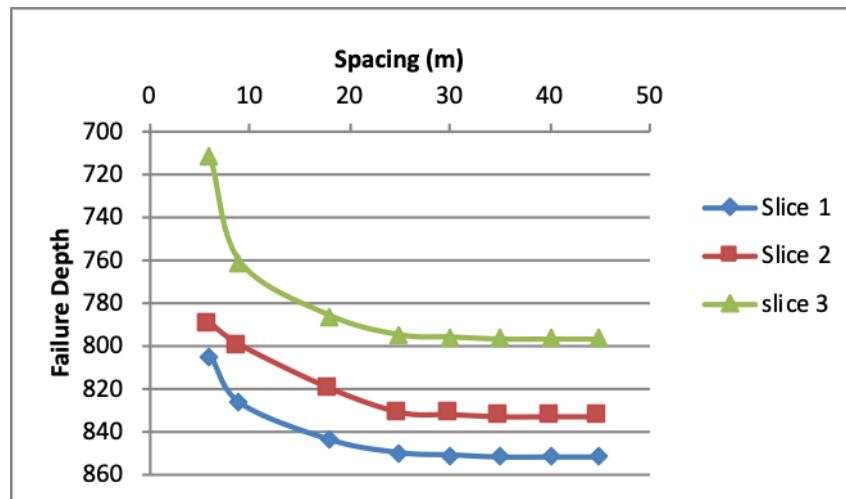


Figure 54 Space Changing effect on failure depth Plot

Figure 54 shows that the less the spacing, the more unstable the all of the tunnels will be, while the longer the distance the stability increases. Also, the failure depth of all tunnels is not changing anymore start from 25 m spacing condition. The constant failure depth at particular spacing indicates all of three individual tunnels are not affected by the presence of the other tunnels. We can maximize stability number, the tunnels should be placed far enough apart to ensure no interaction between the tunnels and that stability number is equal to the single tunnel. In other words, in this condition, all of the tunnels are lose their mechanical connection one to each other.

#### 4.5.4 Stability & Sensitivity Analysis Discussion

From the stability & sensitivity analysis, all of the sample slices are already unstable in shallow depth (on average less than 2 km depth). The karst caves are the suitable analogs for karstic reservoir that have been observed globally in different settings and in Brazil, the estimation of potential Pre-Salt reservoirs are in 3-5 km in-depth which hypothetically believed contains several paleokarst (Agência Nacional do Petróleo, Gás Natural e Biocombustíveis / ANP-National Agency of Petroleum, Natural Gas and Biofuels, Brazil, 2017). Refer to the potential reservoir depth, then the results of the analysis are not the result that we expected. Before it reaches the reservoir depth, the tunnels are already in unstable condition with the possibility of collapse happened, which not good for the industry. The results showed that our model is not fit with the real condition in the reservoir. Some wrong estimations could be the problem in this experiment. As stated before, there are no exact rock properties from each of the caves that could cause a different result. The other thing, during the experiment, our models are assumed as an empty tunnel without any infill (either fluids or breccia), which is in the real condition the karst would be filled with the some materials. Lastly, the software that used is a boundary element method, which only analyzed the boundary of the models that would not count the properties inside the models.

Even though there are still a lot of tentative outputs that found in the whole study, the results still can be used to understanding the pattern of the karst systems and the output can contributes as the first idea to resolve the problems of understanding karst system.

*This page is left blank intentionally*

# Conclusion & Recommendation

## 5.1 Conclusion

The study of 5 caves in Bahia is beneficial as the extra data to learn about the karst system. This study also provides additional information on the geometry, especially the pattern of the shapes and the estimation of stability of the tunnels under specific depths.

This study shows that from LIDAR acquisition, some of the parameters can be extracted. The Geometry analysis showed that in general, two types of tunnel shapes could be seen in all of the 5 caves: Horizontal Ellipse and Vertical Ellipse shapes. Many factors control those shapes, but from this study, it mainly caused by lithology or geology structure aspects. Both, the epigene and hypogene karstification mechanism are hypothetically represented from all of the 5 sample caves and can be proven with the patterns that preserved from the shape analysis. Analysis of the structural features indicates all of the caves show the primary orientation go to N-S and W-E as the secondary orientation. All of the conduit orientation in all caves also controlled by the structure in the surrounding area. This condition caused by both of the conduit orientation and the structural data is having the same direction.

The stability analysis shows that the vertical ellipse tunnels are more stable compared to the horizontal ellipse tunnels. In general, all of the caves are already unstable in shallow depth (on average less than 2 km depth) which not fit with the real pre-salt reservoir condition in Brazil that reaches 3-5 km depth. The input parameters, assumption of the models and the method from the software would be some reasons behind the results. Some more detailed analysis is needed to get a better output. The sensitivity test shows several parameters that would affect the stability: Rock Properties (Rock Mass strength, Rock mass elastic, density), number of tunnels in the system and the distances between multiple tunnels.

Although there are still a lot of tentative outputs that found in the whole study, the results still can be used to understanding the pattern of the karst systems and the output can contributes as the first idea to resolve the problems of an understanding karst system.

## 5.2 Recommendation

This study is only the first step on how to deal with karst problems. Some of the recommendations to expand this study in the future is needed to make all everything sharper. Firstly, the subsurface data acquisition will be helpful since the LIDAR is only capturing until the base level of the cave. By using the subsurface data, the analysis can be broadened, and for the several caves, it will help to see the real base level, which in the surface it is sealed with the sedimentation. Second, the integration with the geochemical and petrography data could give the clear story of the origin of the tunnel shape. Thirdly, there is an interesting part in TOR; the regular spacing maze one that would be interesting to focus on and find the origin. Lastly, the stability analysis can be done with another method. The use of FEM (Finite Element Method) instead of BEM to get more detailed results and also to find a way to put other properties (e.g. Infill materials) into the model would be a better way to get more realistic results.

- [1]. Agar, S.M., Geiger, S., 2014. Fundamental controls on fluid flow in carbonates: current workflows to emerging technologies. *Geol. Soc. Spec. Pub. Lond.* 406.
- [2]. Almeida, DE F.F.M., and Hasui, Y., eds., 1984, *O Precambriano do Brasil* : Sao Paulo, Ed. Edgard Blucher, 377 p.
- [3]. Almeida, De F.F.M., 1977, *O Craton Sao Francisco*: *Revista Brasileira de Geociencias*, Sao Paulo, v.7, p. 349-364
- [4]. Audra, P., Waele, J. De, Pisani, L., & Del, U. (2019). Processes and properties in fractured and karstified carbonate reservoirs.
- [5]. Audra, P., & Palmer, A. N. (2015). Nova Področja speleogenetskih raziskav: Povezava med hidrogeološkimi razmerami, prevladujočimi procesi in tipi jam. *Acta Carsologica*, 44(3), 315–348. <https://doi.org/10.3986/ac.v44i3.1960>
- [6]. Babinski, N.A., Chang, H.K., and Santos, R.C.R., 1989, Hydrocarbon occurrence in Proterozoic Sao Francisco Basin, Brazil (abstract): 28th International Geologic Congress, Abstract, v.1, p 66-67.
- [7]. Baecher G. Christian J. 2003, *Reliability and statistics in geotechnical engineering*, Wiley: London.
- [8]. Basso, M., Kuroda, M. C., Afonso, L. C. S., & Vidal, A. C. (2018). Three-Dimensional Seismic Geomorphology of Paleokarst in the Cretaceous Macaé Group Carbonates, Campos Basin, Brazil. *Journal of Petroleum Geology*, 41(4), 513–526. <https://doi.org/10.1111/jpg.12719>
- [9]. Beekman, F., Badsı, M., van Wees, J.D., 2000. Faulting, fracturing and in situ stress prediction in the Ahnet basin, Algeria a finite element approach. *Tectonophysics* 320 (3-4), 311–329. May.
- [10]. Beskos, D.E., (editor) *Boundary Element Methods in Mechanics*, North-Holland, Amsterdam, 1987
- [11]. Bonfim, L.L.C., Rocha, A.J.D., Moraes Filho, J.C.R., Guimaraes, J.T., Tesch, N.A., Motta, A.C., Souza, G.V.V., and Barral, S.M.Q., 1985, *Projecto Bacia de Irece*: Secretaria das Minas e Energia, Companhia Baianade Pesquisa Mineral, unpublished report, 3 vol.
- [12]. Burchette, T. P. 2012. Carbonate rocks and petroleum reservoirs: a geological perspective from the industry. *Geological Society, London, Special Publications*, 370, 17-37.
- [13]. Carminatti, M., Wolff, B., Gamboa, L. (2008). New exploratory frontiers in Brazil. *World Petroleum Congress*, n. 19, 1-11. Madrid.
- [14]. Cazarin, C. L., Bezerra, F. H., Ennes-silva, R. D. A., Balsamo, F., & Auler, A. S. (2016). Using Analogue Hypogene Karst Systems to Understand the Pre-Salt Carbonate Reservoirs Offshore Brazil \*, 51327.
- [15]. Cornea, N. D., Silver, D., Min, P. (2006). *Curve-Skeleton Properties, Applications and Algorithms*. Rutgers University, New Jersey, USA
- [16]. DOU, Q., SUN, Y., SULLIVAN, C. and GUO, H., 2011. Paleokarst system development in the San Andreas Formation, Permian Basin, revealed by seismic characterization. *Journal of Applied Geophysics*, 75, 379-389.
- [17]. E. Goodman, R. (1989). *Introduction to Rock Mechanics* (Second Edition). Berkeley: John Wiley & Sons.
- [18]. T.A. Cruse and F.J. Rizzo. A direct formulation and numerical solution of the general transient elastodynamic problem, I. *Aust. J. Math. Anal. Appl.*, 22(1):244–259, 1968.
- [19]. Cruz, S. C. P., & Alkmim, F. F. (2006). The tectonic interaction between the Paramirim aulacogen and the Araçuaí belt, São Francisco craton region, Eastern Brazil. *Anais Da Academia Brasileira de Ciencias*, 78(1), 151–173. <http://doi.org/S0001-37652006000100014>
- [20]. Ennes-Silva, R. A., Bezerra, F. H. R., Nogueira, F. C. C., Balsamo, F., Klimchouk, A., Cazarin, C. L., & Auler, A. S. (2016). Superposed folding and associated fracturing influence hypogene karst development in

- Neoproterozoic carbonates, São Francisco Craton, Brazil. *Tectonophysics*, 666,244–259.  
<http://doi.org/10.1016/j.tecto.2015.11.006>
- [21]. Ezhov YA, Lysenin GP, Andreychouk VN, Dublyansky VN (1992) Karst in the Earth's crust. *Sibirskoye otdeleniye Instituta geologii, Novosibirsk*
- [22]. Faybishenko, B., Witherspoon, P., Bodvarsson, G., 2005. Emerging Issues in Fractured-Rock Flow and Transport Investigations: Introduction and Overview, in *Dynamics of Fluids and Transport in Fractured Rocks*. In: Faybishenko, B., Witherspoon, P., Gale, J. (Eds.), 162. American Geophysical Union, Washington, DC, AGU Monograph, pp. 1–11.
- [23]. Hoop, S. De, & Prabhakaran, R. (2018). Report Molengraaff Fund Grant 3D Outcrop Study of Hypogene Karst Caves of Brazil using LIDAR and Drone Imagery
- [24]. Jennings, J. N. 1971. *Karst. An Introduction to Systematic Geomorphology*, Vol. 7. vii+253 pp., 69 figs. M.I.T. Press, Cambridge, Mass., and London
- [25]. Karfulfel, J., and Hoppe, A, 1988, Late Proterozoic glaciation in central east Brazil : synthesis and model : *Palaeogeography, Palaeoclimatology, Palaeoecology*, v.65, p. 1-2
- [26]. Klimchouk, A.B., 2007. *Hypogene Speleogenesis: Hydrogeological and Morphogenetic Perspective*. National Cave and Karst Research Institute, Carlsbad.
- [27]. Klimchouk A (2012) Speleogenesis, hypogenic. In: Culver DC, White BW (eds) *Encyclopedia of caves*, 2nd edn. Elsevier, Chennai, pp 748–765
- [28]. Klimchouk, A.B., 2013. *Hypogene Speleogenesis, Its Hydrogeological Significance and the Role in Evolution of Karst*. DIP, Simferopol (in Russian).
- [29]. Klimchouk AB (2015) The karst paradigm: changes, trends and perspectives. *Acta Carsologica* 44(3):289–313
- [30]. Klimchouk A (2017) Types and Settings of Hypogene Karst. *Research Gate*. DOI: 10.1007/978-3-319-53348-3\_1
- [31]. Lieutier. A. Any open bounded subset of  $R^n$  has the same homotopy type than its medial axis, *Proc. ACM SMI*, 2003.
- [32]. Long, J.C.S., Aydin, A., Brown, S.R., Einstein, H.H., Hestir, K., Hsieh, P.A., Myer, L.R., Nolte, K.G., Norton, D.L., Olsson, O.L., Paillet, F.L., Smith, J.L., Thomsen, L., 1996. *Rock Fractures and Fluid Flow—Contemporary Understanding and Applications*. National Academy Press, Washington, DC, p. 551.
- [33]. Mascarenhas, J.F.M, Pedreira, A, J., Misi, A., Motta, A.C., ad S, J.H.S., 1984, *Provincia Sao Francisco*, in Almeida, de F.F.M., and Hasui, Y., eds, *O precambriano do Brasil : Sao Paulo*, Ed. Edgard Blucher, p.46-122
- [34]. Misi, A., Kyle, J.R., 1994. Upper Proterozoic carbonate stratigraphy, diagenesis, and stromatolitic phosphorite formation, Ireče Basin, Bahia, Brazil. *J. Sediment. Res.* A64,299–310.
- [35]. Misi, A., Kaufman, A. J., Azmy, K., Dardenne, M. A., Sial, A. N., & de Oliveira, T. F. (2011). Chapter 48 Neoproterozoic successions of the Sao Francisco Craton, Brazil: the Bambui, Una, Vazante and Vaza Barris/Miaba groups and their glaciogenic deposits. *Geological Society, London, Memoirs*, 36(1), 509–522.  
<http://doi.org/10.1144/M36.48>
- [36]. Palmer, A., 1991. Origin and morphology of limestone caves. *Geol. Soc. Am. Bull.* 103,1–21
- [37]. Pettijohn, F.J. (1975) *Sedimentary Rocks*. 2nd Edition, Harper and Row Publishers, New York, 628 p.
- [38]. Sauro, F., Zampieri, D., Filipponi, M., 2013. Development of a deep karst system within a transpressional structure of the Dolomites in north–east Italy. *Geomorphology* 184, 51–63
- [39]. Sayago, J., Di Lucia, M., Mutti, M., Cotti, A., Sitta, A., Broberg, K., Przybylo, A., Buonaguro, R. And Zimina, O., 2012. Characterization of a deeply buried paleokarst terrain in the Loppa High using core data and multiattribute seismic facies classification. *AAPG Bulletin*, 96(10),1843-1866.
- [40]. Sokolov DS (1962) Principal conditions of karst development. *Gosgeoltehzdat, Moscow* (in Russian)

- [41]. Sweeting, M.M., 1950. Erosion cycles and limestone caverns in the Ingleborough district (England). *J. Geol.* 115, 63–78.
- [42]. Swinnerton, A.C., 1932. Origin of limestone caverns. *Geological Society of America Bulletin* 43, 663–694.
- [43]. Wu Xinsong, Wei Jianxin, Chang Jianbo, et al. Difficulty and countermeasures in carbonate paleokarst reservoir prediction. *Journal of China University of Petroleum: Edition of Natural Science*, 2009, 33(6): 16–21.
- [44]. Zverev VP (1999) Mass flows of the underground hydrosphere. Nauka, Moscow, pp 96 (in Russian)

Appendix 1 : 5 caves map overview

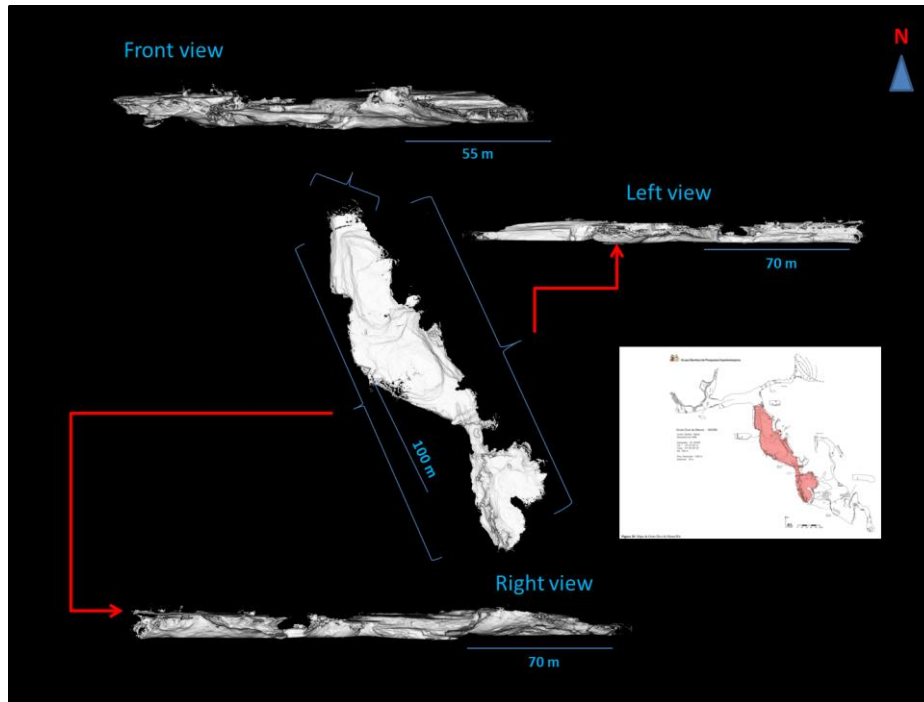


Appendix 2 : Detailed Point Cloud Data

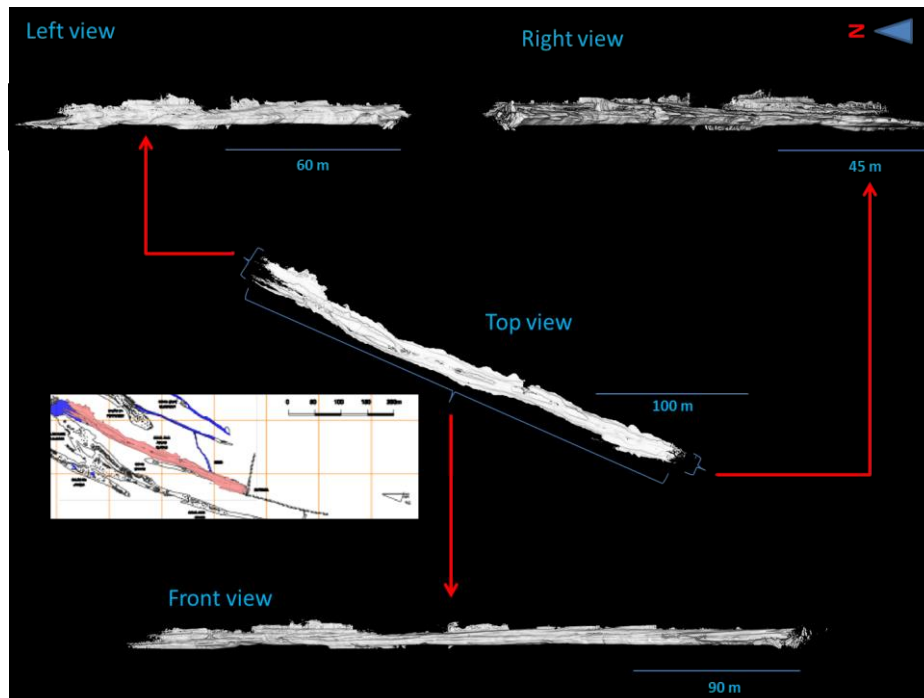
Cave	Total Points
<b>DDM (DDM)</b>	43,391,767
<b>IOI (IOI)</b>	35,911,676
<b>TOR (TOR)</b>	70,957,043
<b>LAP (LAP)</b>	36,239,534
<b>PAX (PAX)</b>	50,295,335

Appendix 3 : Alignment Cave

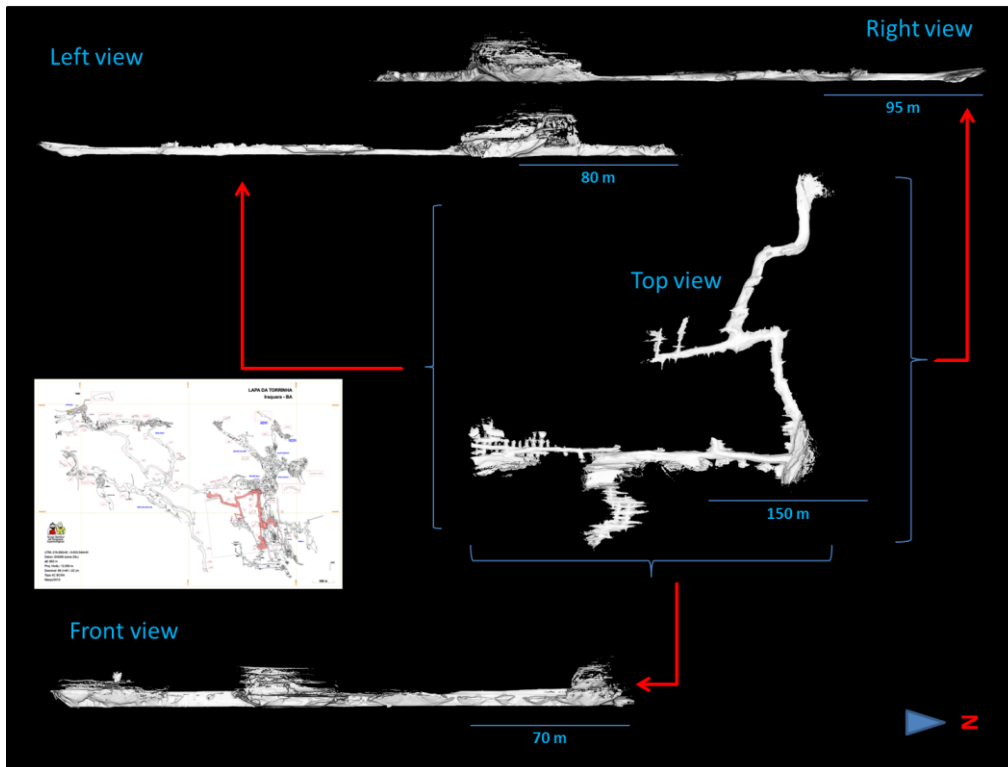
1.DDM



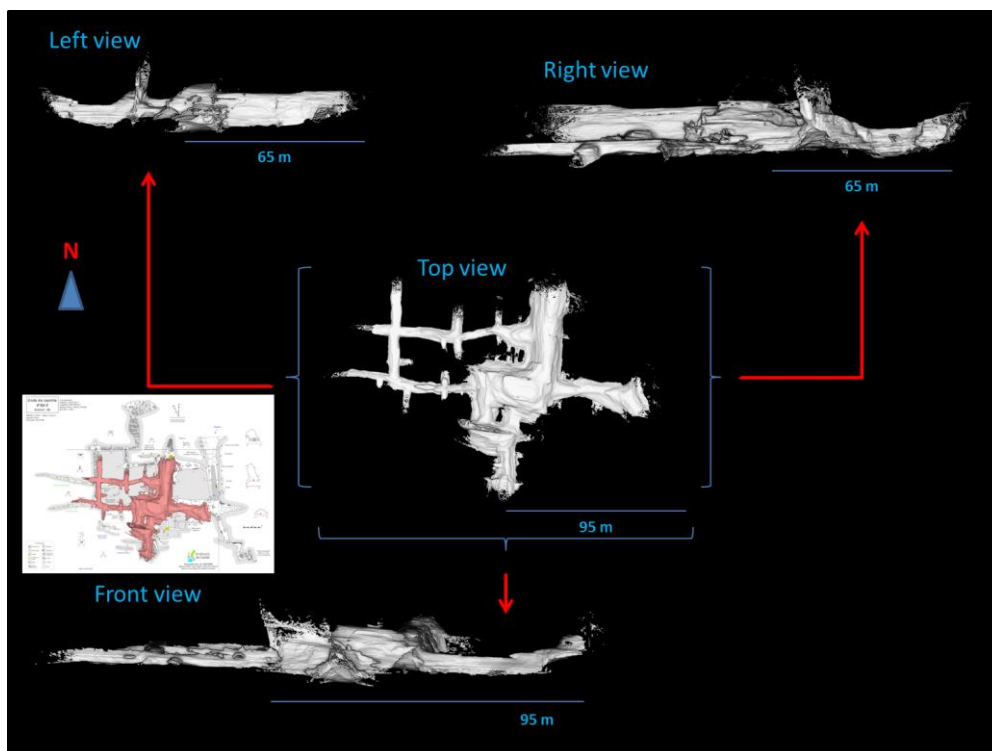
2.IOI



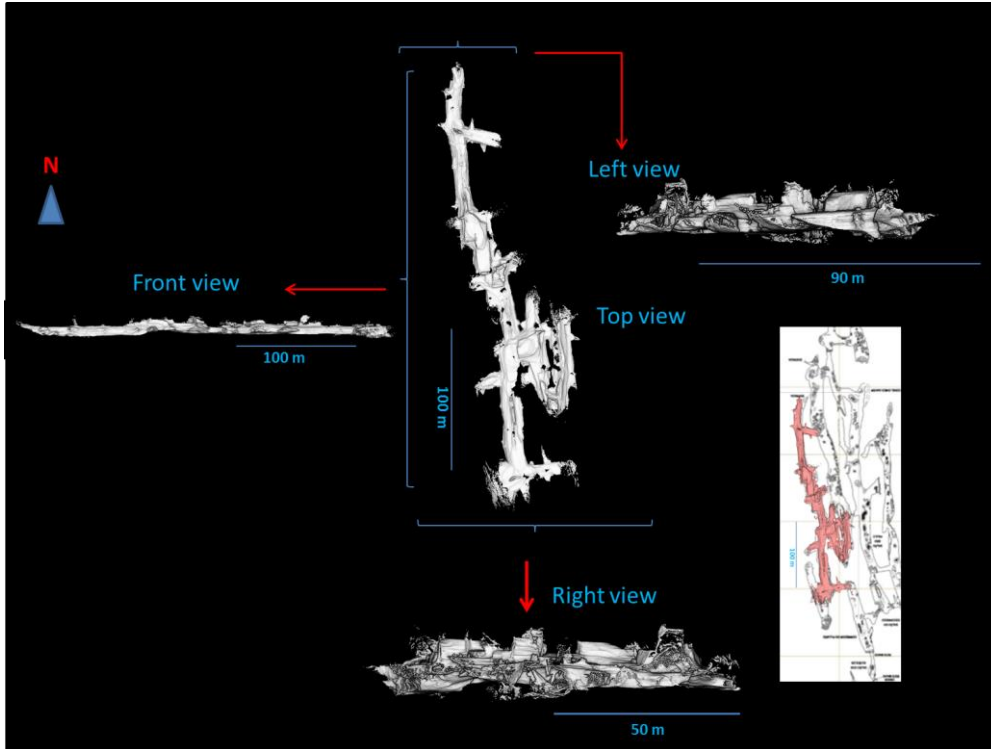
3.TOR



4.LAP



5.PAX



Appendix 4 : Structural Data

DDM					
Fractures	DIP Direction	Dip Angle	Veins	DIP Direction	Dip Angle
	335	90		248	88
	332	90		243	83
	330	90		240	79
	340	90		258	80
	338	90		235	75
	16	90			
	336	90			
	325	90			
	20	90			
	250	90			
IOI					
Fractures	DIP Direction	Dip Angle			
	272	85			
	273	86			
	275	82			
	256	80			
	274	87			
	274	85			
	275	84			
	260	85			
	280	86			
	273	82			
	272	80			
	280	87			
	278	85			
	269	84			
	274	85			
	275	86			
	277	82			
	258	80			
	276	87			
	276	85			
	277	84			
	262	85			
282	86				
275	82				
274	80				
282	87				
280	85				
271	84				

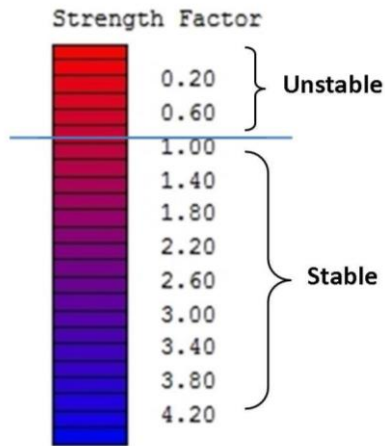
TOR					
	Fractures		Veins	Fractures	
	DIP Direction	Dip Angle		DIP Direction	Dip Angle
	260	90		73	88
	255	90		262	85
	215	90		242	85
	260	90		284	88
	186	90		258	87
	250	90		250	87
	260	90		258	84
	257	90		91	86
	225	90		357	86
	230	90		262	88
	70	90		164	84
	69	90		352	88
	86	90		347	89
	80	90		84	87
	90	90		263	88
	65	90		246	78
	80	90		177	83
	83	90		263	74
	64	90		164	75
	355	90		236	79
	90	90		266	87
	87	90		251	79
	65	90		153	86
	88	90		73	88
	93	90		232	82
	260	90		259	89
	270	90		273	82
	272	90		271	87
	273	90			
	265	90			
	82	90			
	87	90			
	83	90			
	79	90			
	85	90			
	75	90			
	82	90			
	75	90			
	85	90			
	80	90			
	83	90			
	80	90			
	74	90			
	74	90			
	85	90			

LAP					
	DIP Direction	Dip Angle		DIP Direction	Dip Angle
	Fractures	95		90	Fractures
105		90	172	90	
103		90	83	90	
93		90	91	90	
71		90	276	90	
103		90	354	90	
175		90	92	90	
160		90	75	90	
100		90	92	90	
100		90	182	90	
101		90	359	90	
165		90	170	90	
177		90	80	90	
60		90	9	90	
145		90	2	90	
180		90	10	90	
175		90	4	90	
163		90	345	90	
164		90	155	90	
179		90	Veins	DIP Direction	Dip Angle
170		90		92	89
187		90		196	89
75		90		198	87
2		90		97	86
358		90		183	88
278		90		211	85
174		90		98	89
342		90		90	89
345		90		165	85
12		90		345	82
304		90		23	8
276		90			
268		90			
198		90			
201	90				
353	90				
90	90				
352	90				
20	90				

PAX					
	DIP Direction	Dip Angle		DIP Direction	Dip Angle
	Fractures	0		90	Veins
280		90	328	88	
270		90	348	84	
170		90	162	82	
266		90	159	85	
180		90	78	89	
265		90	168	86	
257		90	184	89	
264		90	188	81	
282		90	158	86	
60		90	21	82	
265		90			
256		90			
253		90			
244		90			
253		90			
236		90			
157		90			
253		90			
76		90			
242		90			
259		90			
7		90			
242		90			
232		90			
334		90			
262		90			
68		90			
88	90				
85	90				
86	90				
84	90				
86	90				
89	90				

Appendix 5 : Stability Analysis Contour Plot

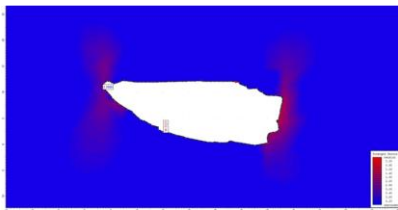
Colour Legends



DDM

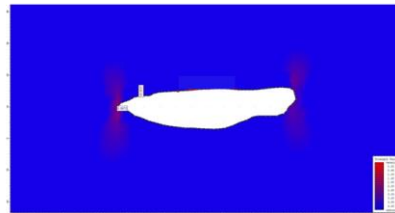
- Slice 3

Real Case  
Failure Depth : 472 m



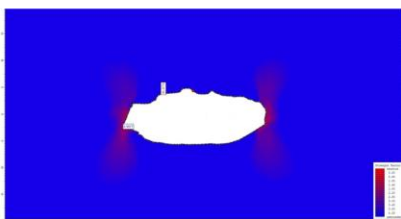
- Slice 4

Real Case  
Failure Depth : 451 m



- Slice 6

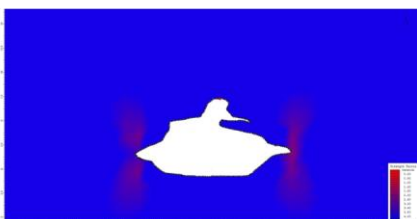
Real Case  
Failure Depth : 331 m



IOI

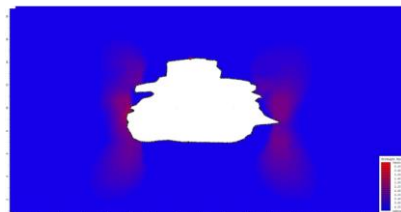
- Slice 6

Real Case  
Failure Depth : 173 m



- Slice 7

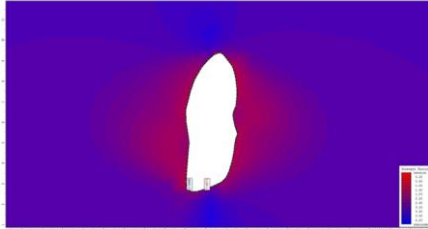
Real Case  
Failure Depth : 169 m



**TOR**

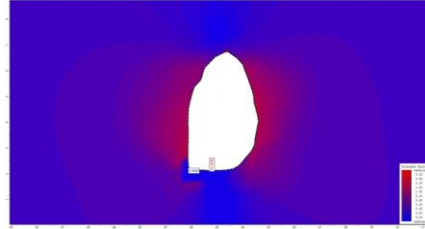
• Slice 1 (Maze Part)

Real Case  
Failure Depth : 856 m



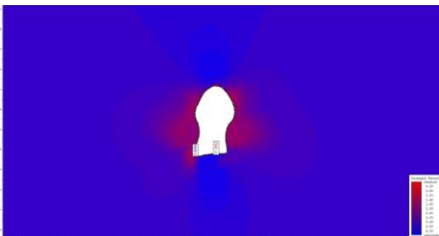
• Slice 2 (Maze Part)

Real Case  
Failure Depth : 827 m



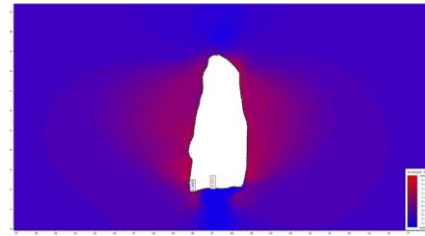
• Slice 3 (Maze Part)

Real Case  
Failure Depth : 793 m



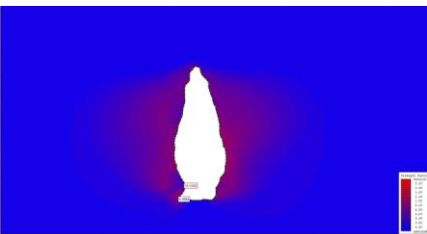
• Slice 1.3 (Eastern horizontal part)

Real Case  
Failure Depth : 762 m



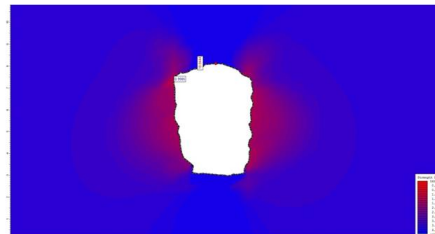
• Slice 1.5 (Eastern horizontal part)

Real Case  
Failure Depth : 568 m



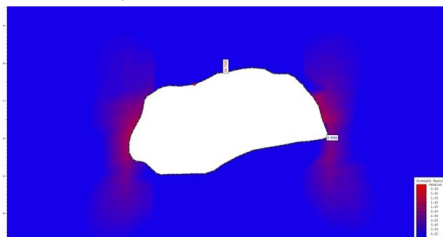
• Slice 3.1 (Eastern horizontal part)

Real Case  
Failure Depth : 632 m



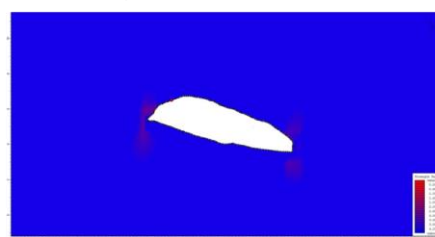
• Slice 4 (Western vertical part)

Real Case  
Failure Depth : 382 m



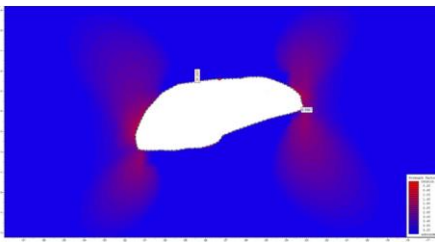
• Slice 1 (Middle Horizontal Part)

Real Case  
Failure Depth : 167 m



•Slice 3 (Western Horizontal Part)

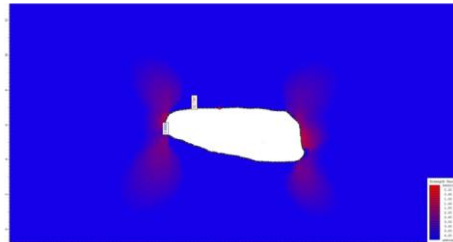
Real Case  
Failure Depth :446 m



LAP

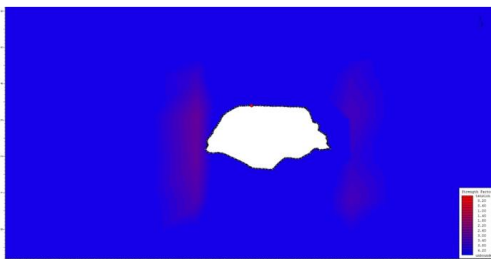
•Slice 2 (Top Western Part)

Real Case  
Failure Depth :384 m



•Slice 4

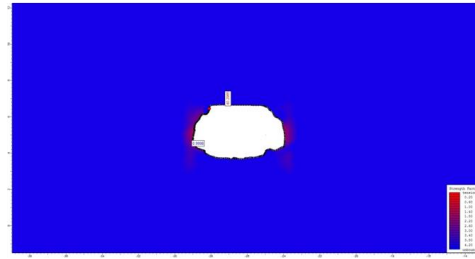
Real Case  
Failure Depth :291 m



PAX

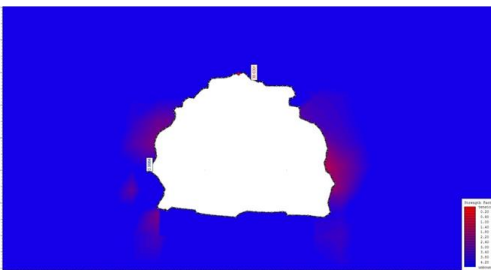
•Slice 6

Real Case  
Failure Depth :337 m



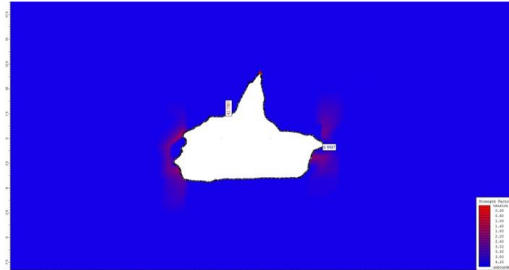
•Slice 3

Real Case  
Failure Depth :335 m



•Slice 6

Real Case  
Failure Depth : 304 m



Appendix 6 : Tornado Plots

